Ophir Flomenbom

Heterogeneous Walkers in Rich Environments

Preface

In this book, we study several stochastic processes that are new variants of known problems: the dynamics of a random walker in heterogeneous environments and the dynamics of many interacting walkers in a quasi one dimensional system (a channel). We present various methods of solving these systems; several of these are new and exciting and should supply ways of solving related problems. We show that these processes exhibit new and interesting behaviours.

In the variant of a random walker in a diverse environment, we address the dynamics of an anomalous walker in a constantly changing environment. Our result shows that when the anomaly has two different origins, namely, two different mechanisms, they compete each other, and eventually only one mechanism for anomaly wins.

In file dynamics (sometimes called single file dynamics or the exclusion process), we study here several new files. Firstly, we find that the dynamics of heterogeneous walkers have a unique scaling law for the mean square displacement (*MSD*) of a walker in the file: $MSD \sim t^{\mu}$ where $\mu=(1-\gamma)/[2/(1+a)-\gamma]$, γ is associated with the heterogeneity in the system and the power a is associated with the scaling law of the initial conditions of the walkers. This scaling law is very different than the known behaviour in the basic Brownian files, where, $MSD \sim t^{1/2}$.

We then show that anomalous walkers in a file are richer in behaviours. We solve both files of synchronized anomalous walkers and independent anomalous walkers. We show how the anomaly influence on the dynamics that are naturally slow in such a system, and moreover, that independent anomalous walkers in a file actually form clusters defining a phase transition.

We think that the results in this book can help both mathematical scientists in biology, chemistry and physic, since the derivation of the results are rigorous and new, and the results are important and original, yet this book can also help experimentalists in these fields, since the results are applicable for many systems. The processes studied in this book are based on papers that we have written in the years 2008-2011.

Ophir Flomenbom, Spring 2011

Table of contents

I. A single walker in rich environments

I.a. Introduction for walks in heterogeneous environments

The statistical properties of random walks have long been used for explaining processes in physics, chemistry and biology [1.1-1.15]. For example, the motion of molecules in solution or in gas phase is important in chemistry when describing reactions [1.2, 1.3], and in biology when describing biological processes in living cells [1.4, 1.15]. Diffusion is also used for describing the properties of glassy materials in physics [1.7]. Extensions of diffusion models are also common; for example, diffusion is used in describing dynamics of energy of molecules [1.3], the price of stocks in the stock exchange [1.16], and so on.

Among the basic properties of a random walker is the scaling of its effective jumping time probability density function (JT-PDF) for individual jumps; this function, $\psi(t)$, determines many of the important statistical quantities of the random walk, like the scaling of mean square displacement (*MSD*) with time, the propagator of the process, and so on [1.2-1.9]. For example, when each microscopic jump of a symmetric random walker is taken from an exponential JT-PDF with a rate k, $\psi(t) = ke^{-kt}$, the *MSD* of the random walker is proportional to the time the process has been going on, $MSD \approx Dt$. This is the well-known diffusive behavior (Brownian motion, e.g. [1.1-1.9]), and the proportionality constant D is the diffusion constant (and is proportional to k). In a continuous model with a coordinate x, the Brownian dynamics follows

the diffusion equation for the PDF for staying at point *x* at time *t*, $P(x,t)$; this equation follows, $\partial_t P(x,t) = D\partial_{xx} P(x,t)$. Indeed, the diffusion equation has the standard scaling for the *MSD*, $MSD \approx Dt$. Nevertheless, many processes in condensed phase take place in heterogeneous environments, and this affects the equation of motion (in a discrete form or a continuous form), and consequently the standard linear scaling of the *MSD* with time is not observed. A model for such a process is a diffusion process composed of diffusion with a diffusion coefficient that changes randomly each microscopic jump; the equation of motion is an average over all the random values of the diffusion coefficient: $< \partial_t P(x,t) >=< D\partial_{xx} P(x,t) >$. The discrete counterpart of this model, a random walker in a heterogeneous system, is defined when taking the value of *k* to depend on the local environment, such that it is also a random quantity taken from a particular PDF *p*(*k*), e.g. [1.9]. We present this model in the next chapter and show that indeed this simple model for a continuous time random walker in a random environment can lead to a multi-exponential form for $\psi(t)$. Moreover, for certain choices of *p*(*k*), this model can lead to slow diffusion, i.e. the random walker's mean square displacement scales sub-linearly with time, and $\psi(t)$ decays as an inverse power law with an infinite mean, i.e. $\psi(t) \sim t^{-1-\mu}$, $0 < \mu \leq 1$. This anomalous behavior is termed subdiffusion. This result is indeed known in the literature of random walks and stochastic processes, e.g. [1.7], and was related during the years with process in chemistry, biology, and physics, such as, diffusion in glassy materials [1.7], processes in fractals [1.5, 1.7, 1.9], reactions [1.2-1.4], processes in biological systems [1.2-1.4], etc.

Here, we analyze a previously un-described variant of a random walk in a random environment: a symmetric *anomalous* random walker in a random environment. (The analysis is based on our work in this field [1.17]). Specifically, the underlying microscopic jumping times

are distributed as an inverse power law with an infinite mean, parameterized with a power β and a rate k:

$\varphi(t;k)\sim\frac{k}{(1+kt)^{1+\beta}}$.

The environment, i.e. the distribution in the rate k, $p(k)$, follows a power law function with a power γ,

$p(k)=\frac{1-\gamma}{\tilde{k}}\left(\frac{\tilde{k}}{k}\right)^{\gamma}$.

We calculate the effective JT-PDF for individual jumps of such a system, $\psi(t)$, obtained when averaging $\varphi(t;k)$ with $p(k)$,

$\psi(t)=\int_0^\infty p(k)\varphi(t;k)dk$,

and show that in this system $\psi(t)$ exhibits a transition in the rule for the power that governs the scaling of $\psi(t)$. $\psi(t)$ always decays as a power law with an infinite mean,

$\psi(t)\sim t^{-1-\mu}$, $\quad 0<\mu\leq 1$,

yet the formula for $\mu(\gamma,\beta)$ changes in a critical point, $\beta=1-\gamma$. Importantly, this is an indication for a change in the mechanism that controls the dynamics. When β is larger than $1-\gamma$,

$\mu=1-\gamma \quad ; \quad \beta>1-\gamma$,

meaning that the collective effect of the environment is the mechanism that controls the dynamics. In this regime, the collective effect of an environment made of many slow regions leads to a slower subdiffusion than the subdiffusion due to the individual jumps. When β is smaller than $1-\gamma$,

$\mu=\beta \quad ; \quad \beta<1-\gamma$,

and the slow individual jumps control the dynamics. Within the model solved here, the phenomenon is independent of the dimension of the system, but vanishes when the power β is distributed also, where in such a case, very slow dynamics are seen.

We suggest several systems that are possibly related with the reported phenomenon: dynamics on a network made of heterogeneous fractals, dynamics of a file of particles in a channel, and dynamics in crowded biological cells. These results are important in applications, yet also when studying anomalous processes mathematically, since its indicate that there are (at least) two distinct models that show anomalous behavior and these models compete each other. We also suggest several extensions of the current work; for example a process with dynamical environment such that β is a process. We think that scientists in mathematical physics and mathematical chemistry can find these results important, yet also scientists in biophysics and chemistry and physics dealing with applications that exhibit anomalous dynamics.

This chapter is presented in three main paragraphs: the introduction, part I.a., part I.b. that presents the known model for an exponential random walker in a random environment leading to slow diffusion, and part I.c. presenting the new variant of this model, where an anomalous walker moves in a random environment, indeed showing a competition among different mechanisms for anomaly. Part I.c. also considers several extensions of the new model and presents a discussion about the results, and concludes this chapter.

I.b. A normal walker in rich environments

A well known result in stochastic processes expresses the scaling of the *MSD*, $< r^2 >$, of a normal diffusive symmetric random walker as a linear function of the time, $< r^2 > \sim Dt$. In this work, the sign ~ symbolizes asymptotic scaling. The diffusion coefficient, D, can be related to properties of the system: the temperature (or energy) of the solution ($k_B T$, where k_B is the Boltzmann constant), the viscosity of the solution (η), and the particle's size (a_p); the most known scaling is the Einstein-Stokes relation, $D = \frac{k_B T}{a_p \eta}$ e.g. [1.3, 1.6]. The linear scaling of $< r^2 >$ with time is pretty general: it holds in any dimension and may hold also when the environment is heterogeneous (while adjusting the value of D so it reflects average properties of the environment). Yet, there are cases in which the environment leads to a very slow diffusion, locally, and when there are many such slow local regions, the scaling for $< r^2(t) >$ can be slower than a linear function of *t*. This is termed a subdiffusion behavior. A simple microscopic model for subdiffusion originates from a combination of a normal diffusive random walker with an exponential JT-PDF for individual jumps [1.9],

$$\varphi(t;k) = ke^{-kt}, \quad (1)$$

and a random environment that leads to a distribution in *k* with many small *k*s; namely, the value for *k* is a random quantity, and is drawn in each transition from a PDF,

$$p(k) = \frac{1-\gamma}{\tilde{k}}\left(\frac{\tilde{k}}{k}\right)^{\gamma}, \; 0 \le \gamma < 1, \quad (2)$$

and *k* is between zero and $\tilde{k}$, for a finite maximal rate $\tilde{k}$. (The fastest timescale in the system, namely, the largest rate, is finite.). This model of the random environment is also termed a fluctuating environment, a changing environment, or a heterogeneous environment.

For this model, the effective JT-PDF of the random walker, $\psi(t)$, defined with the relation,

$$\psi(t) = \int_0^\infty p(k)\varphi(t;k)dk = \sum_k a_k e^{-kt}, \quad (3)$$

decays as a power law, e.g. [1.9],

$$\psi(t) \sim \frac{\tilde{k}}{(\tilde{k}t)^{1+\mu}} \quad ; \quad \mu = 1-\gamma. \quad (4)$$

A consequence of a heavily tailed $\psi(t)$ is that the scaling for $< r^2 >$ is sub-linear in time, e.g. [1.7],

$$< r^2 > \sim \left(\widetilde{D}_0 t\right)^{\mu}.$$

$\widetilde{D}_0$ is a parameter. This result for the *MSD* is obtained from the general scaling-law for the *MSD* in a CTRW: $< \overline{r^2}(s) > \sim \frac{\bar{\psi}(s)/s}{1-\bar{\psi}(s)}$, where $\bar{g}(s) = \int_0^\infty g(t)e^{-st}dt$ is the Laplace transform of the function *g*(*t*). Note that the Laplace transform of the power law $\psi(t)$ in Eq. (4) follows, $\bar{\psi}(s) \sim 1 - \left(\tilde{k}s\right)^{\mu}$. This model shows how the environment can affect the diffusion, leading to subdiffusion. Here, the reason for the subdiffusion is that there are many regions in which the local rate *k* is very small. As $\gamma \to 0$, the diffusion becomes normal.

The continuous counterpart of this model is written in terms of a distribution of diffusion coefficients, $< \partial_t P(x,t) > = < D\partial_{xx} P(x,t) >$, with the following relation of the *MSD*,

$$MSD = 2\int_0^t < D(\tau) >_{D.C.} d\tau,$$

where the average $<\cdot>_{D.C.}$ is taken over all possible realizations of the random values of the diffusion coefficients. The quantity $< D(\tau) >_{D.C.}$ is calculated from the integral, $< D(\tau) >_{D.C.} \sim \int_0^{\widetilde{D}} De^{-D\tau}p(D)dD \sim \tau^{-\gamma}$, for large values of τ, since *D* is as *k* and so it is taken from Eq. (1), and $p(D)$ is as $p(k)$ in Eq. (2). When using this result in the equation for the *MSD* once sees, $MSD \sim t^{1-\gamma}$, similar with the result of the discrete counterpart.

Indeed, there are other models with an anomalous result for the *MSD*, such as due to special geometries or special types of interactions of the diffusing molecules. Nevertheless, the current model is simple and clear, and presents a reference basic model for the occurrence for anomalous dynamics and a power-law JT-PDF. We use an extension of this model in the next chapter for studying the diffusion of an anomalous particle in a heterogeneous environment.

I.c. An anomalous walker in rich environments

I.c.1. The model and its solution

Here, we extend the known simple model for normal diffusion in a random environment, and introduce a model that involves *subdiffusion* in a random environment. We consider a model in which the jumping times for individual jumps are distributed according to a power law PDF, with a particular scaling power β,

$$\varphi(t;k) = (2+\beta)\frac{k}{(1+kt)^{1+\beta}} \quad ; \quad 0 < \beta \leq 1. \qquad (5)$$

In each jump the parameter *k* is drawn from the PDF in Eq. (2); namely, the random environment is modeled in the same way as before. The calculations compute the effective JT-PDF found from the integral equation,

$\psi(t) = \int_0^\infty p(k)\varphi(t;k)dk.$

$\psi(t)$ represents a process that is renewal, since the random times are drawn independently each jump, in a heterogeneous environment, since the environment in modeled with $p(k)$. The solution for $\psi(t)$ in the current model follows,

$$\psi(t) = \tilde{k}\left(\frac{1}{\tilde{k}t}\right)^{2-\gamma}\int_0^{\tilde{k}t}\frac{s^{1-\gamma}}{(1+s)^{1+\beta}}ds. \quad (6)$$

For large $\tilde{k}t$, the integral, $I \equiv \int_0^{\tilde{k}t}\frac{s^{1-\gamma}}{(1+s)^{1+\beta}}ds$, is approximated with the sum of three integrals,

$$I \approx \int_0^{C_1} s^{1-\gamma}ds + \int_{C_1}^{C_2}\frac{s^{1-\gamma}}{(1+s)^{1+\beta}}ds + \int_{C_2}^{\tilde{k}t} s^{-\gamma-\beta}ds. \quad (7)$$

In Eq. (7), we take the constant C_1 as a small number and the constant C_2 as a large number (smaller than $\tilde{k}t$). The first integral in right hand side (RHS) of Eq. (7) is correct up to order $o(C_1)$ and the third integral in the RHS of Eq. (7) is correct up to order $o(1/C_2)$. The second integral in the RHS in Eq. (7) is always a positive constant, and we denote it by C_3.

Equation (7) has the solution,

$$I \approx \frac{C_1}{2-\gamma} + C_3 + C_2^{1-\gamma-\beta}\frac{\left(\tilde{k}t/C_2\right)^{1-\gamma-\beta}-1}{1-\gamma-\beta}. \quad (8)$$

When $1-\gamma = \beta$,

$$I \approx \frac{C_1}{2-\gamma} + C_3 + \ln(\tilde{k}t/C_2) \equiv A + \ln(\tilde{k}t).$$

For large *t*, the outcome of the integral *I*, Eq. (7), depends on the sign of $1-\gamma-\beta$:

$$I \approx \begin{cases} \frac{C_1}{2-\gamma} + C_3 + \frac{C_2^{1-\gamma-\beta}}{\gamma+\beta-1} & 1-\gamma < \beta \\ A + \ln(\tilde{k}t) & 1-\gamma = \beta. \\ \frac{\left(\tilde{k}t\right)^{1-\gamma-\beta}}{1-\gamma-\beta} & 1-\gamma > \beta \end{cases}$$

Consequently, the expression for $\psi(t)$ obeys,

$$\tilde{k}^{-1}\psi(t) \sim \begin{cases} \left(\tilde{k}t\right)^{-2+\gamma} & 1-\gamma < \beta \quad (9.1) \\ \frac{A+\ln(\tilde{k}t)}{\left(\tilde{k}t\right)^{1+\beta}} & 1-\gamma = \beta \quad (9.2) \\ \left(\tilde{k}t\right)^{-1-\beta} & 1-\gamma > \beta \quad (9.3) \end{cases}$$

Equations (9.1) and (9.3) are correct for large $\tilde{k}t$ independent of $1-\gamma$ and β, where exactly in the point $1-\gamma=\beta$, $\tilde{k}^{-1}\psi(t)$ obeys Eq. (9.2). These equations form the main mathematical results in this chapter.

Numerical simulations.- Equations (9) predict a transition in the rule for the power that governs the scaling law of the effective JT-PDF for a subdiffusive random walk in a random environment. This occurs when $1-\gamma=\beta$. It is very simple exemplifying this transition in a simulation. Here, we perform kinetic Monte Carlo simulations. We first draw a random number for determining the parameter values of the JT-PDF and then use this in the JT-PDF and draw a random jumping time. This procedures is performed over and over again (10^7 random times are drawn for each curve). The way random numbers are drawn here is by using the typical way for generating random numbers from a power-law PDF: given the PDF in Eq. (2), we generate a random rate when using the formula, $k=\tilde{k}x^{\frac{1}{1-\gamma}}$, where x is a random number distributed uniformly in a unit interval. Figures 1-3 present the results from these simple numerical simulations. Each figure shows result for the average JT-PDF $\psi(t)$ from a particular simulation specified with particular values of γ and β. We take for β, $\beta=0.25, 0.5, 0.75$, and each value of β is conjugated with two different γs, one that leads to Eq. (9.1) and another that leads to Eq. (9.3); $\gamma=0.625, 0.01$ for $\beta=0.75$ shown in Fig. 1, $\gamma=0.75, 0.25$ for $\beta=0.5$ shown in Fig. 2, and $\gamma=0.875, 0.25$ for $\beta=0.25$ shown in Fig. 3. The transition is apparent in all cases.

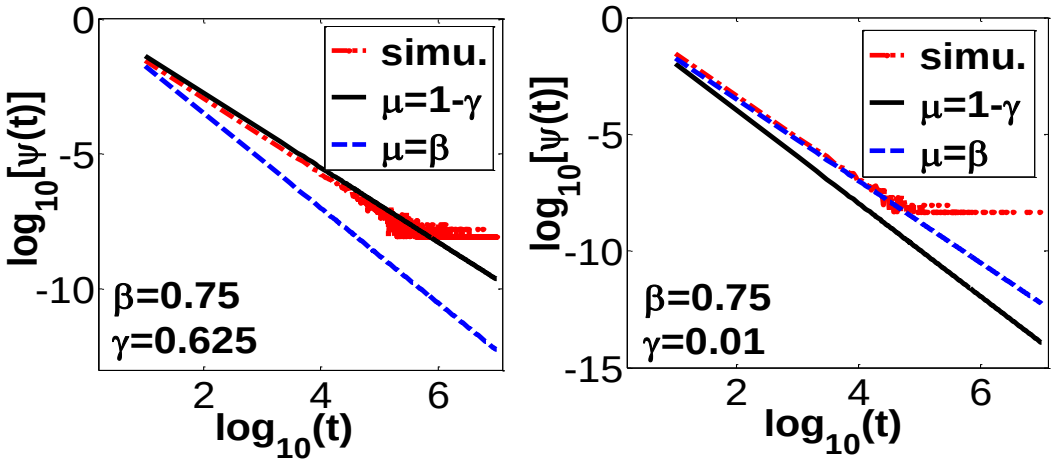

Fig 1 A log-log plot of the effective JT-PDF versus time (dashed-dotted symbols), obtained from kinetic Monte Carlo simulations with 10^7 events. In each panel, shown are also two curves that correspond to power-laws, $t^{-1-\mu}$, with different values for μ ($\mu = 1-\gamma$ and $\mu = \beta$). The right panel ($\gamma = 0.01$ and $\beta = 0.75$) shows that the effective JT-PDF scales as the input JT-PDF sincen $1-\gamma > \beta$. The left panel ($\gamma = 0.625$ and $\beta = 0.75$) emphasizes the transition, showing that the scaling of effective JT-PDF is determined by the environment, when $1-\gamma < \beta$. In the inset, '*simu.*' means simulations' results. The parameter $\tilde{k}$ in Eq. (2) is set to unity. The noise at large t in the curves obtained from the simulations is expected for results from stochastic dynamics (at large t).

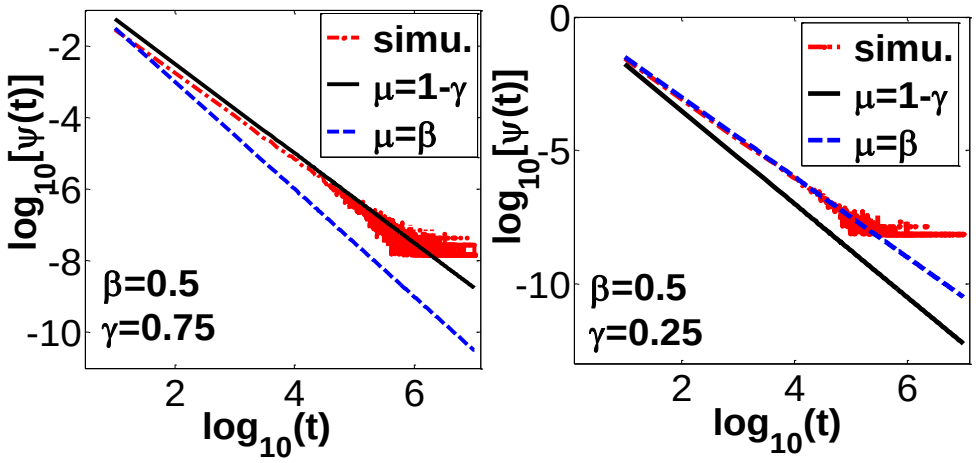

Fig 2 Results from simulations are presented in the same format as in Fig. 1, with different values for γ (= 0.75, 0.25) and β (=0.5). Note that when the environment controls the dynamics (left panel), converge is asymptotic with time.

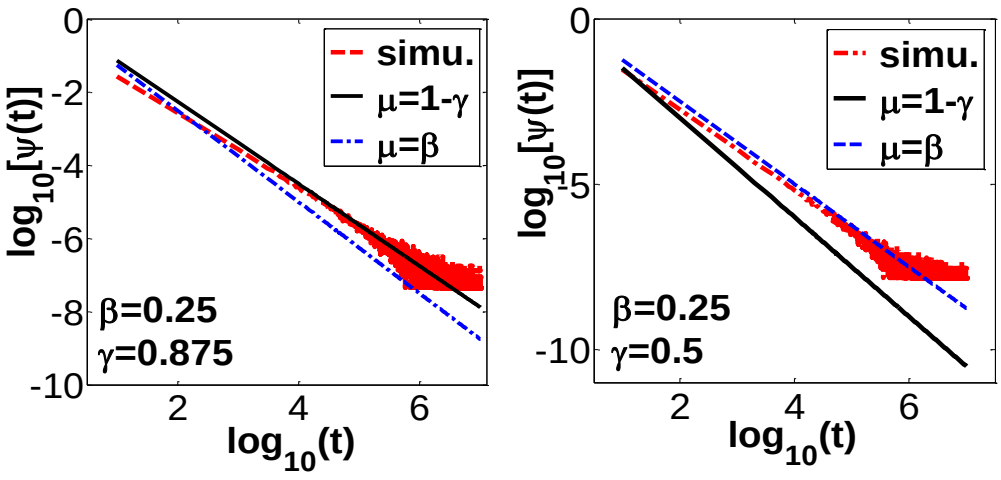

Fig 3 Results from simulations are presented in the same format as in Fig. 1, with different values for γ (= 0.875, 0.5) and β (=0.25). Again, we note that when the environment controls the dynamics (left panel), converge is asymptotic with time.

We note that in the cases where the collective effect of many slow regions determines the scaling of the JT-PDF, the convergence is asymptotic. This is of course an expected behavior. Note also that this transition in the scaling of the effective JT-PDF is independent of the dimension of the system, since the effective JT-PDF for individual jumps is independent of the dimension of the system. The effective JT-PDF depends only on the input local JT-PDF for individual jumps and the heterogeneity in the system, and both, in this model, are independent of the dimension of the system.

I.c.2. ***Extensions, physical explanations, and applicability***

In the previous part, we showed both mathematically and numerically that an anomalous random walker in a diverse environment can diffuse slower than the anomaly for individual jumps when

the environment is diverse. What about a random environment that leads to a distribution in the power β in Eq. (5)? In this case, the environment affects also the value of the power β since, for example, the system has special geometries that are distinct among the sites in the lattice. For such a system, we find that a transition in the scaling law of $\psi(t)$ is not observed, with or without distribution in the parameter *k*, as long as the average over the power β is performed in the range, $\epsilon \leq \beta \leq 1$ (here, $\epsilon \to 0^{+}$). For showing this, we choose two functions as the PDF of the power β. First, when choosing,

$$g(\beta) \sim \beta^{-J} \quad ; \quad 0 \leq J < 1, \tag{10}$$

straightforward calculations give,

$$\psi(t) \sim \frac{k}{(1+kt)^{1+\epsilon}} \left(\frac{1}{\log(1+kt)}\right)^{1-J}, \tag{11.1}$$

and,

$$\psi(t) \sim \frac{\tilde{k}}{(\tilde{k}t)^{1+\epsilon}} \left(\frac{1}{\log(\tilde{k}t)}\right)^{1-J}, \tag{11.2}$$

before and after an additional averaging with $p(k)$ is done, respectively. When choosing,

$$g(\beta) \sim (1-\beta)^{-J},\ 0 \leq J < 1, \tag{12}$$

calculations show that,

$$\psi(t) \sim \frac{k}{(1+kt)^{2}} (\log(1+kt))^{J}, \tag{13.1}$$

and,

$$\psi(t) \sim \frac{\tilde{k}}{(\tilde{k}t)^{2-\gamma}} \left(\log(\tilde{k}t)\right)^{J}, \tag{13.2}$$

before and after an additional averaging with $p(k)$ is performed, respectively. Note that the limit $J \to 0$ should be taken in Eqs. (11), since the results in Eqs. (13) are obtained when exploiting the fact that most of the probability $g(\beta)$ is located near one for, $g(\beta) \sim (1-\beta)^{-J}$.

The above calculations were performed when averaging over the power β and then over the parameter k. We can reverse the order of the averaging, and first average over the parameter k and then over the βs. This order of averaging requires two different integration regimes, as can be seen from Eqs. (9). One must distinguish between the following two different random environments: in one set of random systems, β is in the range, $1-\gamma \leq \beta \leq 1$, whereas in the other set of random systems β is in the range, $0 \leq \beta \leq 1-\gamma$. When starting with Eqs. (9) and performing the restricted averaging with $g(\beta)\sim(1-\beta)^{-J}$, one sees only *one* result for $\psi(t)$ in both averaging regimes, $\psi(t)\sim\frac{\tilde{k}}{(\tilde{k}t)^{2-\gamma}}$. That is, the transition disappears for this choice of $g(\beta)$. Restricted integrations are important when averaging with $g(\beta)\sim\beta^{-J}$. Here, when β is integrated in the range $1-\gamma$ and 1 one sees,

$$\psi(t)\sim\frac{\tilde{k}}{(\tilde{k}t)^{2-\gamma}}, \tag{14.1}$$

yet when β is integrated in the range 0 and $1-\gamma$ one sees,

$$\psi(t)\sim\frac{\tilde{k}}{(\tilde{k}t)^{1+\epsilon}}\frac{1}{[\log(\tilde{k}t)]^{1-J}}. \tag{14.2}$$

Thus, when the environment allows any value of the power β, the value of γ cannot affect the scaling of $\psi(t)$, and the transition is not observed. The transition disappears because there are not so few local JT-PDFs with slower exponent β than the exponent $1-\gamma$ related with the environment. Nevertheless, when the range of allowed β values is correlated with the value of γ, different scaling in $\psi(t)$ can be obtained depending on the shape of $g(\beta)$ and on the integration range for β. This is an artificial transition because one must prepare the system to fulfill the condition on β, and this special preparation leads to a different scaling in $\psi(t)$. The physical origin of this transition is the same as in the *fixed* β case.

How can we interpret the reported phenomenon? Looking on Eq. (9.1), we note that it scales as Eq. (4). Also, Eq. (9.3) scales as Eq. (5). Namely, the effective JT-PDF follows the slower mechanism: anomaly resulting from individual jumps or resulting from the slow environment. We also conclude that the local subdiffusive dynamics competes with the anomaly resulting from the heterogeneity in the system. When local jumps are very slow compared with the anomaly originated from the environment ($1-\gamma>\beta$), the diffusion does not depend on the environment's heterogeneity. However, when the environment becomes very slow ($1-\gamma<\beta$), the individual transitions are, effectively, exponentially distributed from the environment 'perspective', and only the exponent of $p(k)$ enters in the scaling of $\psi(t)$ like the average over $\varphi(t;k)$ is performed with an exponential JT-PDF for individual jumps.

What are the implications of the reported transition? There are several systems that can be described with this model. For example, a continuous time random walker in a branched lattice. The branches are fractals with the same spectral dimension (the spectral dimension determines the power β [1.10]), but differ in conductivity; namely, each fractal is characterized with a rate for individual jumps drawn from $p(k)$. Here, the statistical properties of the random walker can be tuned when adjusting, for example, the distribution of the fractals' conductivity while keeping fixed their spectral dimension.

Looking beyond a single random walker model, we predict that the transition reported here will be found also in a renewal file of many sub-diffusive hard spheres in a quasi one-dimensional channel (where collisions are elastic) [1.11-1.14]. In the renewal sub-diffusive file, all particles attempt a jump together and the JT-PDF for individual transitions obeys Eq. (5) with a random diffusion coefficient *k* drawn from the PDF in Eq. (2) for each jump. We conjecture

that a transition in the scaling of the *MSD* of a sphere in this file will be observed when the collective effect due to the PDF in diffusion constants leads to a slower dynamics relative to the anomaly related with the heavily tailed JT-PDF for individual jumps. As shown here, these two factors are not additive, yet compete each other. The next chapter study anomalous files.

The last example that we consider here is diffusion in living cells [1.13]. The cell content is dense, and diverse (the density fluctuates in space and time). It is well known that crowding is observed in the cell due to its high density content; that is, slow dynamics are observed. In what follows, a model that takes into account both the slow individual jumps and the heterogeneity in the environment is considered. This model exhibits the phenomenon reported in the previous part of this chapter, and may be found constructive in the analysis of the dynamics in living cells. It can be related for any entity that diffuses in the cell, say, a protein or DNA molecule.

We consider local dynamics governed with an exponential JT-PDF,

$$\varphi(t;k) = ke^{-kt}. \tag{15}$$

The rate k (the local diffusion constant) is parameterized with an energy barrier, and obeys the Kramers relation for a reaction rate, e.g. [1.3],

$$k = k_0 e^{-\Delta/\tilde{\Delta}}. \tag{16}$$

Since the local composition of molecules that form the local environment changes across the system, the energy barrier Δ is distributed; here, we choose the following PDF, $f(\Delta)$, for describing the distribution in Δ:

$$f(\Delta) = \frac{1}{\tilde{E}} e^{-\Delta/\tilde{E}}. \tag{17}$$

This model, Eqs.(15)-(17), gives a power-law JT-PDF:

$$\psi(t;k_0)=\int f(\Delta)\varphi(t;k(\Delta))d\Delta\sim\frac{k_0}{(k_0t)^{1+\beta}} \qquad ; \qquad \beta=\frac{\tilde{\Delta}}{\tilde{E}}.$$

The parameter $\tilde{\Delta}$ is related with the temperature, and so it is a constant in the cell environment. The parameter k_0 can be related with the local 'friction' and thus can be distributed on the level of the cell. The parameter $\tilde{E}$ determines the scale of the local barriers. Although, it can be argued that both $\tilde{E}$ and k_0 can be distributed, $\tilde{E}$ is more likely not to change much in a changing environment, since the nature of the interactions between molecules in the cell is pretty much similar regardless of the local density of the molecules, and that the local density affects mainly the local friction, namely, the prefactor, k_0. When modeling the distribution in the k_0 with a PDF of the form of Eq. (2), i.e.,

$$p(k_0)=\frac{1-\gamma}{\tilde{k}}\left(\frac{\tilde{k}}{k_0}\right)^{\gamma},\ 0\le\gamma<1, \tag{19}$$

we find a model for subdiffusion in a diverse environment that can lead to the transition predicted in Eqs. (9),

$$\tilde{k}^{-1}\psi(t)=\int p(k_0)\psi(t;k_0)dk_0\sim\begin{cases}\left(\tilde{k}t\right)^{-2+\gamma} & 1-\gamma<\beta \quad (20.1)\\ \frac{A+\ln(\tilde{k}t)}{(\tilde{k}t)^{1+\beta}} & 1-\gamma=\beta \quad (20.2)\\ \left(\tilde{k}t\right)^{-1-\beta} & 1-\gamma>\beta \quad (20.3)\end{cases}.$$

Thus, crowding can affect the dynamics in the cell in more than one way; first, it is the reason for an effective anomalous dynamics for individual jumps since the dynamics are possible only when many 'microscopic' slow events occur, and then, it may affect the scaling of the effective JT-PDF, when there are enough 'very dense' local environments (causing a distribution in k_0). Finally, we note that although the anomalous behavior can be terminated with a threshold in time, the above analysis refers to a situation in which the anomaly is observed in a time window important to the biological activity.

Concluding Remarks.- In this chpater, we considered a *subdiffusive* continuous time random walker (characterized by a power β) in a heterogeneous environment (characterized with a power γ). We showed that this system exhibits a transition in the scaling law of its effective JT-PDF, $\psi(t)$. $\psi(t)$ decays as a power law, $\psi(t)\sim\frac{1}{t^{1+\mu}}$, yet μ obeys two different formulae. When $1-\gamma > \beta$, $\mu=\beta$, yet when $1-\gamma < \beta$, $\mu = 1-\gamma$. The transition in the scaling of $\psi(t)$ reflects the competition between two different mechanisms for subdiffusion: subdiffusion resulting from the heavily tailed JT-PDF for microscopic jumps, and subdiffusion resulting from the collective effect of an environment made of many slow local regions. These two different mechanisms for subdiffusion are not additive, yet compete each other. The reported transition is dimension independent, but disappears when the power β is also distributed in the range, $0 < \beta \leq 1$. We introduced several systems that can show this phenomenon and thus can be related with, e.g. dynamics of a file of hard particles in a channel, and diffusion in dense living cells.

Many extensions of the mathematical model presented here are possible. We present one such possibility for concluding this chapter. The model is an anomalous walker with a power β and a random system modeled with $p(k)$. The new thing here is that the power β is a process also; say, for simplicity, the power has two different values $\beta_{\pm}$, with independent dynamics. We expect seeing interesting behaviors of this model depending on the dynamics in the powers $\beta_{\pm}$. Such a model can reflect a situation where the properties of the molecule under investigation are controlled externally, and this is the reason for the dynamics in $\beta_{\pm}$.

II. Normal File dynamics: Many walkers in a channel

II.a. File dynamics

II.a.1. Introduction

The *basic* process of file dynamics is a diffusion problem of N Brownian hard spheres in an open quasi one dimensional channel. (Here, a Brownian hard sphere is a normal random walker that interacts with the other first adjacent walkers like elastic interactions.) All the particles in the channel have the same diffusion coefficient D. The limit in which the system's length, L, goes to infinity is taken, along with the demand the particles' density, $\rho=\rho_0=N/L$, is on average a constant, so $N=L/\Delta$, for a microscopic length scale Δ. This process is sometimes called single file dynamics or an exclusion process. Here, it is simply termed file dynamics.

The statistics of a given particle in the file, termed the tagged particle, are known for the simple file since 60s (1960s) [2.1-2.9]. (Hereafter, the tagged particle is identified with the coordinate r, and is the middle particle in the file, where N is odd). The probability density function (PDF) of the tagged particle is asymptotically a Gaussian in the coordinate r, with a variance (termed also the mean square displacement, *MSD*) that scales as the square root of time,

$$P(r,t|r_0)\sim(4Dt)^{-\frac{1}{4}}\exp\left\{-\frac{(r-r_0)^2}{\sqrt{4Dt}}\right\} \quad ; \quad D\to D\rho^{-2}.$$

This result is special since the *MSD* scales like the square root of the time rather than linear with the time, like in Brownian motion. The PDF $P(r,t|r_0)$ was first obtained in Ref. [2.2] in the mathematical literature, for stochastic dynamics. In the physical community, file dynamics were

studied with several approaches, including mappings [2.7-2.9], correlation function calculations [2.6, 2.14], and numerical simulations [2.10-2.14]. Recent studies provided complementary characterizations of the dynamics in the file. For example, studies showed that the file's motion is correlative [2.15], the fluctuations in the particles' density obey a diffusion equation [2.6, 2.15], the velocity auto-correlation function has a negative tail [2.14], and that a file of spheres is normal in higher dimensions [2.6]. For a deterministic file with momentum exchange upon collisions, the tagged particle's PDF is also a Gaussian, yet with a variance that scales like the time [2.3]. File dynamics has also been associated with monomer dynamics in a large liner polymer: both systems share a similar scaling law for the mean square displacement of the tagged particle [2.23, 2.28].

File dynamics has attracted a lot of attention in recent years (since the 1990s) in the context of diffusion within confined structures [2.24-2.30]. Examples include diffusion within biological and synthetic pores, and in porous materials, of water, ions, proteins, and organic molecules [2.24, 1.15]. Diffusion along 1D objects, such as the motion of motor-proteins along filaments [1.15]. And even in the context of conductance in nano-wires [2.31].

Still, in many of these real-world systems, one, or several, of the basic conditions that define the *basic* single file process can break down. For example, real-world systems are finite, and this affects the results, as a steady state regime is seen [2.20]. Other modifications useful in describing real-life problems include files that have particles that are passing each other with a constant probability upon collision [2.16-2.19], or files that have particles that interact with the channel and are subject to an external (say, periodic) field [2.12].

In this chapter and in the next one, we present several new files that we studied in a series of recent papers [1.12-1.14, 2.32]: heterogeneous files, renewal-anomalous-heterogeneous files and anomalous files of independent particles. In each case, we present solutions for the file both using mathematical calculations and numerical simulations. Each case exhibits interesting behaviors that are richer than that of a basic file and of files mentioned above. In each case, we relate the model with possible real-life systems. This particular chapter deals mainly with files that have normal dynamics.

II.a.2. Definition of normal heterogeneous files

Heterogeneous files are files that allow both distributions in diffusion coefficients and in the initial density of the particles. Namely, the initial particles' density law scales with the distance l from the origin like,

$$\rho(l) = \rho_0(l/\Delta)^{-a} \quad ; \quad 0 \le a \le 1. \qquad (1)$$

Indeed, $\rho(l)$ in Eq. (1) is the initial density of the file, where the particles are initially positioned at,

$x_{0,j}$=sign(j)Δ$|j|^{1/(1-a)}$,

for $|j| \le M$, $N=2M+1$. Consequently, the initial number of particles n as a function of the length l obeys, $n = (l/\Delta)^{1-a}$. Among the possible realistic choices for a particle-distance law (e.g. an exponential, a Gaussian, or a power-law), the one that affects the dynamics is a power-law, where this is a conclusion from our results and calculations presented in this chapter.

In addition with an initial distribution that is not fixed, the particles' diffusion coefficients are distributed according to a PDF; here, we choose,

$$W(D) = \frac{1-\gamma}{\Lambda}\left(\frac{D}{\Lambda}\right)^{-\gamma}, \quad 0 \le \gamma < 1, \qquad (2)$$

where Λ is the fastest diffusion coefficient in the system and is finite. Again, we show that $W(D)$ is a limiting distribution in the sense that only when there are many small diffusion coefficients around the origin, the heterogeneity affects the dynamics of the particles in the file, where otherwise the results of the basic file are seen with an effective diffusion coefficient.

II.b. Scaling laws for heterogeneous files

II.b.1. Scaling laws for simple files

One of the fundamental results in transport processes states that the particle's mean square displacement for free diffusion (i.e. the Brownian motion: a single particle random walk in an unconfined geometry without traps) is linear in time (for any dimension): $< r^2 >_{\text{free}} \sim \mathrm{D_0 t}$, e.g. [1.1]. This scaling is equivalent with the square root scaling of the average of the absolute displacement with the time, $< |r| >_{\text{free}} \sim \sqrt{\mathrm{D_0 t}}$. For hard spheres in a channel, a slower propagation rate for a tagged particle is expected since for reaching a net distance l, the file's particles (in the relevant direction) must 'cooperate', and all move in the direction of the propagation. Namely, the tagged particle's evolution is a result of a cooperative motion of the file's particles. We use these arguments in deriving scaling laws for the mean absolute displacement (*MAD*) in a simple file. We start when choosing $< |r| >_{free}$ for the natural length scale in the system. Then, we compose the argument of the scaling function from both $< |r| >_{free}$ and $1/n^{\mu}$ where n is the number of particles in the covered interval, and μ is an unknown power. We set the scaling function not a decreasing one, since when increasing the

number of particles that should cooperate, it is harder achieving cooperation from all of the random walkers. Thus, we write,

$< |r| > = f\left(\frac{<|r|>_{free}}{n^{\mu}}\right)$.

$< |r| >_{\text{free}}$ is the upper bound on the diffusion for the tagged particle, so for $n = 1$, $< |r| >=< |r| >_{\text{free}}$. Thus, we need to take a linear scaling function,

$$< |r| > \sim \frac{1}{n^{\mu}} < |r| >_{free}. \quad (3)$$

Note that n is a function of $< |r| >$ and not of $< |r| >_{\text{free}}$, since the number of particles in the actual covered distance is counted. Now, for the standard file dynamics, the particles' density is fixed, and $n \sim r$, and the *MAD* follows , $< |r| > \sim \frac{1}{(\rho < |r| >)^{\mu}} (Dt)^{1/2}$, and consequently,

$$< |r| > \sim \rho^{-\mu/(1+\mu)} (Dt)^{1/[2(1+\mu)]}. \quad (4)$$

For obtaining the known scaling law for a standard single file, $\mu = 1$, so the general scaling law for the mean absolute displacement of a tagged particle in a system of hard spheres with a constant density follows,

$$< |r| > \sim \frac{1}{n} < |r| >_{free}. \quad (5)$$

Note that μ is a positive number when the density is not fixed and is bound from above with unity, since this is the result of a constant density file (we consider density laws that have a finite maximal value). Since Eq. (5) is for a file with a constant density, $\rho = \rho_0$, we find:

$$< |r| > \sim \sqrt{< |r| >_{free} / \rho_0}. \quad (6)$$

Equation (6) is a general result in file dynamics, in the sense that it holds for many types of basic dynamics: Brownian dynamics, renewal-anomalous dynamics, Newtonian dynamics, etc. Now, we conclude from the above derivation and Eq. (6) in particular that the result, $< |r| > \sim \rho_0^{-1/2} (D_0 t)^{1/4}$, for a tagged particle in a basic file is associated with three factors: (1) the

requirement that the free particle mean absolute displacement scales as, $< |r| >_{\text{free}} \sim (D_0 t)^{\frac{1}{2}}$, (2) the requirement for 'cooperation' from the other particles in the length $< |r| >$ that scales as one over the number of particles in the covered length, and (3) the condition of a constant particles' density.

II.b.2. Scaling laws for files with scaled density

We can write down also a formula for the *MAD* for a file with initial density law that follows Eq. (1), yet this is based on results from different calculations, since the value of μ is not known. Namely, the calculations of the scaling laws are limited for files that have the property that any segment in the file has the density $\rho = \rho_0$, and this of course is not the case when the density is not fixed. Still, since the density scales with the distance, it is possible and sensible writing a scaling law for the middle particle in the file; this scaling law follows,

$$\rho_0 < |r| > \sim \left(\rho_0 < |r| >_{free}\right)^{\frac{1+a}{2}}. \qquad (7)$$

Although Eq. (7) is obtained when using in Eq. (3), $= \frac{1-a}{1+a}$, set for matching the result for the *MSD* from calculations of Brownian file's PDFs and scaling-laws [see the discussion around Eqs. (30)-(31)], Eq. (7) indeed generalizes the *MSD* obtained from these calculations, since it addresses also dynamics that are not Brownian.

Now, Eq.(1) is the initial density, yet during the process the distances between particles change. So, without care, each particle in the system will become a free particle, at long times. For handling this scenario, yet still capturing the effect caused by the not-fixed initial density, we define the length L^*, as the length in which the effect is tested. In this length, the initial distances between adjacent particles increases for remote particles from the tagged one, placed on the

origin. Outside this distance, we have a constant density, $\rho^* = \frac{1-a}{\Delta}(L^*/\Delta)^{-a}$. So, we have here a process of particles' spreading: the particles in the denser area spread outside into the periphery, where there, the dentistry is smaller. The diffusion of the tagged particle in this spreading process follows Eq. (7). Note that outside the area of length $2L^*$, the file has much fewer particles and the density is much smaller than of a file with a constant density of, $\rho_0 = \frac{1}{\Delta}$. The above is presented in Fig. II.1 that shows the expected *MSD* in a file with a density that is not fixed in an interval L^*, together with curves for the *MSD* in constant density files with ρ_0 and ρ^*. In this figure, the red curve is the expected *MSD* for a file with *a=1/3* in Eq. (1). We expect observing the effect for several orders of magnitude, in a time span among the first arrow and the third arrow in the figure (the locations of the arrows depend on the value of L^*). The 'trust' upper time $t_{u.b.}$ (the time indicated with the third arrow) is found from, $D_0 t_{u.b.} = (L^*)^2$, and this is the time it takes a free particle reaching the distance L^*. Results from simulations are presented in II.b.4 and indeed coincide with Eq. (7), and with the curves presented in Fig. II.1.

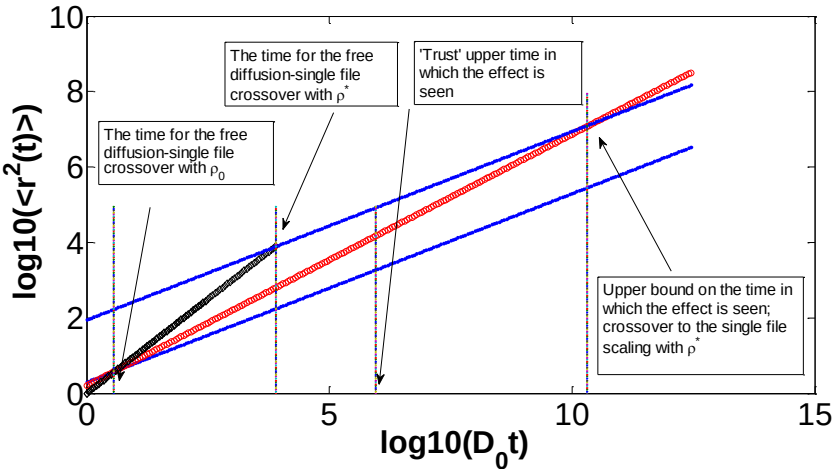

Fig II.1 The MSD in a file with a density that is not fixed in an interval of length L^*. See text for discussion.

II.b.3. Scaling laws for heterogeneous files

In this paragraph, we derive a scaling law for $<|r|>$ in a heterogeneous file with a constant density. We start with the following set of relations,

$$<|r|> = <|r|>_{free}/n = \Delta^{1/2}<|r|>^{1/2}_{free} \approx \Delta^{1/2}[D(<|r|>_{free})t]^{1/4}. \quad (8)$$

Equation (8) and Eq. (5) are similar: n is the number of particles in the cover length, yet $<|r|>_{\text{free}}$ is the *MAD* of a free particle with a *modified diffusion coefficient*, $<|r|>_{\text{free}} \approx [D(<|r|>_{free})t]^{1/2}$. $D(<|r|>_{free})$ should reflect the fact that in an interval of length $<|r|>_{free}$ in the actual file, there is a typical diffusion coefficient that represents all the particles in this length, since we have substituted one for many. Clearly, $D(<|r|>_{free})$ is among the slowest diffusion coefficients in the interval of length $<|r|>_{free}$. Still, it should represent a bunch of slow particles, and not merely the slowest one. For estimating $D(<|r|>_{free})$, we first derive the PDF of the smallest diffusion coefficient, D_{min}, among n particles, denoted as $f(D_{min}, n)$. Since the diffusion coefficients of the particles are drawn independently, this PDF obeys,

$$f(D_{min}, n+1) = W(D_{min})\left(\int_{D_{min}}^{\Lambda} W(D)dD\right)^n. \quad (9)$$

$W(D_{min})$ is the PDF that the slowest diffusion coefficient has a value of D_{min} and the integral to the power of n is the probability that all the other particles have diffusion coefficients that are larger than D_{min}. A normalization constant doesn't affect the following calculations, and it is omitted. Using Eq. (2) in Eq. (9), we find (for $n \gg 1$),

$$f(D_{min}, n+1) \approx (D_{min}/\Lambda)^{-\gamma} e^{-n(D_{min}/\Lambda)^{1-\gamma}}. \quad (10)$$

Equation (10) has the typical form of a PDF in extreme value statistics [2.33]. We use this PDF for linking a typical small diffusion coefficient and n. For this, we look on the exponential factor in the PDF, $e^{-n(D_{min}/\Lambda)^{1-\gamma}}$, and notice that only when the condition, $n(\widetilde{D}_{min}/\Lambda)^{1-\gamma} = 1$, is met,

a large probability can be assigned for small values of D_{min}. Solving for $\widetilde{D}_{min}$, we find, $\widetilde{D}_{min} = \Lambda n^{-1/(1-\gamma)}$. Using $\widetilde{D}_{min}$ in Eq. (10), we find,

$$f(\widetilde{D}_{min}, n) \approx \Lambda^{-1} n^{\gamma/(1-\gamma)}. \quad (11)$$

We define the typical value for the slowest particles in the interval of n particles ($n \gg 1$), denoted as $\widetilde{D}_n$, as one over the PDF $f(\widetilde{D}_{min}, n)$,

$$\widetilde{D}_n \equiv 1/f\,(\widetilde{D}_{min}, n) \approx \Lambda n^{-\gamma/(1-\gamma)}. \quad (12)$$

For using $\widetilde{D}_n$ in Eq. (8), we need the scaling of the number of particles n in $< |r| >_{free}$ with time. For this we use the equation:

$$< |r| >_{free} \sim \sqrt{\widetilde{D}_n t} \sim \sqrt{n^{-\gamma/(1-\gamma)} t} \sim \sqrt{< |r| >_{free}{}^{-\gamma/(1-\gamma)}\ t}\ , \quad (13)$$

since, $< |r| >_{free} \sim n$. Solving Eq. (13) for $< |r| >_{free}$ and using $n \sim < |r| >_{free}$, we see,

$$n \sim t^{\frac{1-\gamma}{2-\gamma}}. \quad (14)$$

Using Eq. (14) in Eq. (12), we have, $\widetilde{D}_n \sim n^{\frac{-\gamma}{1-\gamma}} \sim t^{\frac{-\gamma}{2-\gamma}}$, and when substituting this relation in Eq. (10), we have,

$$\langle |\ R_d\ | \rangle = \tau^{\frac{1-\gamma}{2(2-\gamma)}} \quad ; \quad \tau = \rho_0^2 \Lambda t. \quad (15)$$

In Eq. (15), $R_d = \rho_0 r_d$. Equation (15) is the scaling for the *MAD* in a file of heterogeneous walkers with a constant initial density, namely, for *a=0*. In a file with a density that is not fixed, the file's density doesn't scale with the distance in the sense that a given interval of length l taken from the file at different locations along the file has a different density of particles. Thus, any scaling law for such a file must rely significantly on known results. Discussion about this point is presented around Eq. (7) and Eqs. (30)-(31).

Scaling law analysis enables generalizing the results for files with different kinds of dynamics. We consider in what follows heterogeneous-deterministic files. A deterministic file is

a file in which the particles are Newtonian and each particle is assigned an initial velocity $\pm v$ with equal probability. In a simple deterministic file, the PDF of a tagged particle is a Gaussian with a variance that scales linearly with time. What is $\langle | R_d | \rangle$ when the value $| v |$ is drawn from a PDF of the form of Eq. (2) with equal probability for any direction? Starting from Eq. (8), we find,

$$\langle | R_d | \rangle = (\Delta^{-1} | \tilde{v} | t)^{\frac{1-\gamma}{2-\gamma}}, \qquad (16)$$

where $| \tilde{v} |$ is a characteristic velocity in the system. Equation (16) is calculated in a similar way with the analysis of this paragraph. Equation (16) shows that as $\gamma \to 1$ the deterministic file freezes and as $\gamma \to 0$ the file behaves like a simple deterministic file.

II.c. PDFs in normal files

In this part, we calculate PDFs in simple files, and in heterogeneous files. The dynamics are Brownian in all cases. We show that the PDF of a walker in the file is always a Gaussian with a variance that scales like,

$$\rho_0^2 < r^2 > \sim (\rho_0^2 \Lambda t)^{(1-\gamma)/(2c-\gamma)} \quad ; \quad c = 1/(1+a). \qquad (17)$$

This result for the MSD generalizes the results obtained from scaling laws in the sense that it is correct also for files with initial density that is not fixed.

II.c.1. PDFs in simple files, and files with scaled density

The diffusion equation for the particles' PDF $P(\boldsymbol{x}, t \mid \boldsymbol{x_0})$ in a simple file obeys a diffusion equation (for point particles):

$$\partial_t P(\boldsymbol{x}, t \mid \boldsymbol{x_0}) = D \sum_{j=-M}^{M} \partial_{x_j x_j} P(\boldsymbol{x}, t \mid \boldsymbol{x_0}), \tag{18}$$

with the initial condition,

$$P(\boldsymbol{x}, t \to 0 \mid \boldsymbol{x}_0) = \prod_{j=-M}^{M} \delta(x_j - x_{0,j}) \qquad ; \qquad x_{0,j} = \mathrm{sgn}(j)\Delta|j|^{1/(1-a)}. \tag{19}$$

Here, Δ is a microscopic length, and $0 \le a < 1$. The equation of motion is accompanied with a set of boundary conditions defining the nature of the interactions in the file: each pair of adjacent particles in the file obeys a reflecting boundary condition upon encounters,

$$[\partial_{x_j} P(\boldsymbol{x}, t \mid \boldsymbol{x_0}) - \partial_{x_{j+1}} P(\boldsymbol{x}, t \mid \boldsymbol{x_0})]_{x_j = x_{j+1}} = 0 \quad ; \qquad -M \le j < M-1, \tag{20}$$

which simply means that the adjacent particles bounce towards their territories when collide. The joint multi-walker PDF is calculated from the Bethe ansatz [2.34]. The Bethe ansatz is the {k}-space, $\{k\}=k_{-M},\ldots,k_M$, integrand of the Fourier transform of the solution (x→k),

$$\hat{P}(\boldsymbol{k}, t \mid \boldsymbol{x_0}) = \frac{1}{N!} \prod_{j=-M}^{M} e^{-ik_j x_{0,j}} e^{-Dtk_j^2} \sum_p e^{ik_j x_j(p)}. \tag{21}$$

Here, the index p contains the permutations of all particles' indices, so the summation is over $N!$ permutations (e.g. $x_j(p^*)=x_i$, for a given p^*, and, $-M \le i, j \le M$).

The joint PDF in $\{x\}$-space is found from Eq. (21),

$$P(\boldsymbol{x}, t \mid \boldsymbol{x_0}) = (4\pi D t)^{-\frac{N}{2}} \sum_p \prod_j e^{\frac{-\left(x_j - x_{o,j}(p)\right)^2}{4Dt}}. \tag{22}$$

We can show that $P(\boldsymbol{x}, t \mid \boldsymbol{x_0})$ is normalized to 1 while performing an integration over the $\{x\}$-space coordinates with the restriction,

$$-\infty \le x_{-M} \le x_{-M+1} \le \cdots \le x_{M-1} \le x_M \le \infty. \tag{23}$$

It is seen from direct calculations for small N values that the restricted integration can be replaced with an unrestricted integration for each particle, i.e., $-\infty \le x_j \le \infty$, j=-M,…, M, when dividing the result with $N!$. Thus, each permutation in the expression for $P(\boldsymbol{x}, t \mid \boldsymbol{x_0})$ is a product of N integrals, each of which is normalized to one, and so each permutation contributes a factor

of $1/N!$. Since there are $N!$ permutations, $P(\boldsymbol{x}, t \mid \boldsymbol{x_0})$ is normalized to one. We will use these points in the following calculations.

PDF for the tagged particle.- For obtaining the PDF for the tagged particle, $P(r, t|r_0)$, $r \equiv x_0$ and $r_0 = 0$, we need to integrate out all the file particles' coordinates except of r, while obeying the above restriction, Eq. (23). This is performed when separating the integrals into left integrals, and right integrals,

$$P(r, t|r_0) = \int_{-\infty}^{x_{-M+1}} dx_{-M} \int_{-\infty}^{x_{-M+2}} dx_{-M+1} \dots \int_{-\infty}^{r} dx_{-1} \int_{r}^{\infty} dx_1 \int_{x_1}^{\infty} dx_2 \dots \int_{x_{M-1}}^{\infty} P(\boldsymbol{x}, t \mid \boldsymbol{x_0})\, dx_M .$$

This $2M$-dimensional integration fulfills Eq. (23). The particles always maintain their order. Similar with the calculations of the normalization constant, we can use r as the upper bounds in all the left integrals, and use r as the lower bounds in all the right integrals. Then, $P(r, t|r_0)$ obeys,

$$P(r, t|r_0) = \frac{1}{C} \prod_{j=1}^{M} \int_{-\infty}^{r} dx_{-j} \int_{r}^{\infty} dx_j \, P(\boldsymbol{x}, t \mid \boldsymbol{x_0}) , \qquad (24)$$

where C is the normalization constant. Equation (24) enables further analysis since it expresses $P(r, t|r_0)$ with a products of separate integrals,

$$P(r, t|r_0) \propto \sum_p \mathrm{e}^{-\frac{1}{r_f^2}[r - r_0(p)]^2} \prod_{j=1}^{M} \int_{-\infty}^{r} dx_{-j}\, \mathrm{e}^{-\frac{1}{r_f^2}[x_{-j} - x_{0,-j}(p)]^2} \int_{r}^{\infty} dx_j\, \mathrm{e}^{-\frac{1}{r_f^2}[x_j - x_{0,j}(p)]^2} . \qquad (25)$$

Here, for notation convenience, we define, $r_f \equiv \sqrt{4Dt}$. (r_f equals $< |r| >_{free}$ for normal diffusion, and it is the natural length scale in the system.) For any permutation p', the faith of each integral over x_j, with $j > 0$, is one of following three possible outcomes (here we use asymptotic analysis of large times and a finite r):

(1) When $(r - x_{0,j})/r_f \to 0$, the integral is approximated with, $\pi/2$.

(2) When $(r - x_{0,j})/r_f \to -\infty$, the integral is approximated with, π.

(3) When $(r - x_{0,j})/r_f \to +\infty$, the integral is approximated with, $\frac{e^{-Y_j^2}}{2|Y_j|}$, where, $Y_j = (r - x_{0,j})/r_f$.

These three possible outcomes are also obtained for any integral over x_j with $j < 0$, when switching the condition-part of cases (2) and (3). For each permutation, we count the number of integrals of each kind (cases (1)-(3) above), and then calculate the total of all permutations' results. Counting the important permutations that contribute for $P(r,t|r_0)$ in Eq. (25) is the intriguing part in the calculations of this PDF. Yet, once we manage identifying and actually counting these permutations, we can perform similar calculations also for heterogeneous files. This is the reason that we spell out these calculations here.

We start the analysis of Eq. (25) when analyzing $P(r,t|r_0)$ for small values of r. Here, small r values are such that, $|r| \leq r_f$. We define *ordered-permutations*, denoted with $\{p_o\}$, and these permutations have all initial coordinates, $\{x_{0,j}(p_o)\}_{j=1}^{M}$, positive, when j is positive, and so they are on the right of r, and all the initial coordinates, $\{x_{0,-j}(p_o)\}_{j=1}^{M}$, negative, when $-j$ is negative, and are thus located on the left of r. Figure II.2 illustrates such a possible permutation. Now, since the tagged particle is the middle particle, and r is small, many ordered-permutations exist. In fact, there are $(M!)^2$ such permutations. There are $M!$ internal permutations of the left initial conditions and $M!$ internal permutations of the right initial conditions, starting from the 'perfectly' ordered permutation, $p_o = 1$: $x_{0,j}(1) = \Delta j$ for every j. All such $(M!)^2$ permutations of the 'perfectly' ordered permutation lead to the same result of the integrals in Eq. (25), since the integrals are independent of each other. For small r, only cases (1) and (2) are relevant for the ordered permutations. Each ordered permutation gives a constant independent of r, which gives, $\left(\frac{1}{2}\right)^{2r_f}$. So, we find that for the ordered-permutations, Eq. (25) is reduced, and reads: $\left(\frac{1}{2}\right)^{2r_f} \sum_p e^{-\frac{1}{r_f^2}[r-r_0(p)]^2} \sim \left(\frac{1}{2}\right)^{2r_f} \frac{1}{C} \int_{-\infty}^{\infty} e^{-\frac{1}{r_f^2}[r-\Delta p]^2} dp = \left(\frac{1}{2}\right)^{2r_f}$.

That is, the contribution of ordered permutations to Eq. (25) is a constant independent of r.

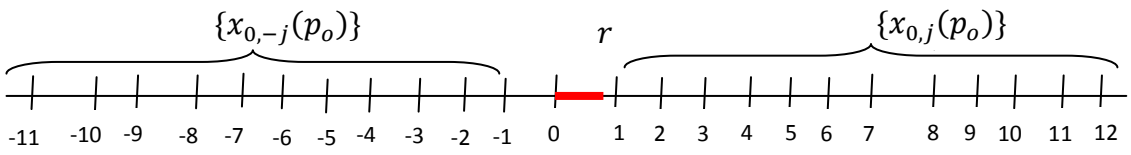

Fig II.2 An illustration of an ordered permutation. Shown are a realization of the initial conditions, with, $x_{0,j}(p_o) = \Delta j$, and the value of r (in red). Each tick represents a particle at the initial stage of the process.

Thus, for $(M!)^2$ ordered permutations from the possible $(2M)!$ permutations in Eq. (25), the small r limit contributes a constant. There are still $4^M(M!)^2$ permutations in which the initial conditions are not ordered. For calculating these permutations, we perform the following calculations: we start with the perfectly ordered permutation, and choose m initial coordinates from the left-M-initial coordinates, and choose m initial coordinates from the right-M-ordered initial coordinates, and switch the sets. For each switch, there are the 'standard' $(M!)^2$ internal permutations all resulting in the same result (that we still need calculating for each switching protocol). We distinguish among the following switching protocols:

- The chosen initial-coordinate is within the distance r_f from r: $\left|r - x_{0,j}(p)\right| \leq r_f$
- The chosen initial-coordinate is at a distance larger than r_f from r: $\left|r - x_{0,j}(p)\right| > r_f$

Using these options, we find that there are 4 possibilities for each switch, with the following results:

- The contribution from switching an initial coordinate within the distance of r_f from r with an initial coordinate within the distance of r_f from r from the other side, that is,

  $x_{0,j}(p) \leftrightarrow x_{0,-i}(p)$; $r + r_f - x_{0,j}(p) > 0$ and $r - r_f - x_{0,-i}(p) > 0$,

  gives approximately the result of the ordered permutations discussed above, that is, a constant independent of r.

- The contribution from permutations in which both initial coordinates that are switched are at a distance larger than r_f from r (in opposite direction), that is,

  $x_{0,j}(p) \leftrightarrow x_{0,-i}(p)$; $r + r_f - x_{0,j}(p) < 0$ and $r - r_f - x_{0,-i}(p) < 0$,

  is small relative to the contributions from the switching protocols in (26) discussed in the next case.

- The important case is when an initial coordinate within the distance of r_f from r is switched with an initial coordinate from the other side (right-left switch or left-right switch) that its distance to r is larger than r_f:

  $x_{0,j}(p) \leftrightarrow x_{0,-i}(p)$; $r + r_f - x_{0,j}(p) > 0$ and $r - r_f - x_{0,-i}(p) < 0$, (26.1)

  or,

  $x_{0,j}(p) \leftrightarrow x_{0,-i}(p)$; $r + r_f - x_{0,j}(p) < 0$ and $r - r_f - x_{0,-i}(p) > 0$. (26.2)

  In what follows we calculate the contributions from these permutations.

Using the results of case (3) above, we find that the switching protocols (26.1)-(26.2) contribute to Eq. (25) terms of the following form:

$$P(r,t|r_0) \propto (M!)^2 \sum_{z=1}^{n(r_f)} \sum_{q=1}^{n(r_f)-z} S_z S_q \prod_{j=1}^{z} \frac{e^{-\left[Y_j(p)\right]^2}}{|Y_j(p)|} \prod_{i=1}^{q} \frac{e^{-\left[Y_{-j}(p)\right]^2}}{|Y_{-j}(p)|}. \quad (27.1)$$

$n(r_f)$ in the upper bounds in Eq. (27.1) is the number of particles in r_f. In a file with a density law obey Eq. (1),

$n(r_f) \sim {r_f}^{1-a} \sim t^{\frac{1-a}{2}}$.

In Eq. (27.1), S_z is the combinatorial factor,

$$S_z = \binom{M-\rho r_f}{z}\binom{\rho r_f}{z},$$

counting the number of ways to perform the switching protocol for z coordinates. Equation (27.1) has two combinatorial factors: S_z is associated with the switching protocol of Eq. (26.1) and S_q is associated with the switching protocol of Eq. (26.2). Each combinatorial factor is associated with a product of Gaussians resulting from calculating the integrals of case (3): S_z is associated with the product, $\prod_{j=1}^{z} e^{-[Y_j(p)]^2}/|Y_j(p)|$, and S_q is associated with the product $\prod_{i=1}^{q} e^{-[Y_{-j}(p)]^2}/|Y_{-j}(p)|$. Note that, in principle, the arguments of the Gaussians depend on the indices z and q, $Y_j(p) = Y_j[p(z)]$, and $Y_{-j}(p) = Y_{-j}[p(q)]$. Yet, the actual form of $Y_j(p)$, in the context of Eq. (27.1), should obey,

$$Y_{\pm j}(p) = \frac{r \mp \bar{R}}{r_f},$$

where $\bar{R}$ is a very large number. The reason is that $x_{0,\pm j}(p)$ in, $Y_{\pm j}(p) = \big(r - x_{0,\pm j}(p)\big)/r_f$, should reflect all the M coordinates from the left (right) of r for $x_{0,j}(p)$ $[x_{0,-j}(p)]$, and for this we must use an average quantity, say, $\bar{R}$ $(-\bar{R})$, and this quantity is positive (negative) and large when M is large, since $\bar{R}$ is proportional to M. We will use this point in the final step of deriving $P(r,t|r_0)$.

Now, we look on Eq. (27.1) and note that we can replace S_z and S_q with their maximal value, and write an upper bound for Eq. (27.1):

$$P(r,t|r_0) \leq \frac{1}{C}\sum_{\tilde{p}} e^{-\sum_{j=-n}^{n} Y_j(\tilde{p})^2 + \ln\left(|Y_j(p)|\right)}, \qquad (27.2)$$

where $\tilde{p}$ goes over all the permutations in Eq. (27.1) (about n^2 permutations). Equations (27) are the major results of this sub-chapter.

Starting from Eqs. (27), the limit of many particles, where M is much larger than r_f, is considered. Then, the symmetric term, $z = q = n/2$, dominates the sum in Eq. (27.1), and we

find:

$$P(r,t|r_0) \propto \left(M!\, S_{\rho_0\sqrt{Dt}}\right)^2 \prod_{j=1}^{n} \frac{e^{-\left[Y_j(p)\right]^2-\left[Y_{-j}(p)\right]^2}}{|Y_j(p)||Y_{-j}(p)|}$$

$$\lesssim \left(M!\, S_{\rho_0\sqrt{Dt}}\right)^2 e^{-\rho_0 n\left[Y_+^2+Y_-^2+\log|Y_-||Y_+|\right]}. \qquad (28)$$

In Eq. (28), we use, $Y_{\pm j}(p) \to Y_\pm = (r \mp \bar{R})/r_f$, relying on the fact that all the initial coordinates in $\{Y_j\}$ are at a distance of, at least, r_f from r, yet the average of all of these is much larger, and proportional to $\pm M$. Thus, the leading term for the PDF of the tagged particle reads,

$$P(r,t|r_0) \propto e^{-n\frac{{r_d}^2}{4Dt}} \sim e^{-{R_d}^2/\tau^{(1+a)/2}} \quad ; \quad R_d = \rho_0 r_d, \qquad (29)$$

since $n(r_f) \sim {r_f}^{1-a} \sim t^{\frac{1-a}{2}}$. Eq. (29) should appear with a logarithmic correction in the exponent. For large values of r, $|r| \geq r_f$, there are always n initial coordinate in the left of r (say $r > 0$). This gives rise to a correction term, $e^{-\frac{\rho_0(|r|-\sqrt{4Dt})^3}{4Dt}}$, which multiplies the result of any permutation. (This term holds for a constant density.) But, the switching analysis is the same as discussed above. The correction term is important only when $|r| \geq 3r_f$, yet the PDF at such distances is of the order of $o(10^{-6})$.

Equation (29) gives the *MSD* for a file with a density that is not fixed (for the middle particle):

$$< {R_d}^2 > \sim \tau^{(1+a)/2}. \qquad (30)$$

Since, $\tau^{(1+a)/2} = \left(< {R_d}^2 >_{free}\right)^{(1+a)/2}$, Eq. (30) is written also in a form of a *MAD*,

$$< |R| > \sim < |R| >_{free}{}^{(1+a)/2},$$

and from this equation we conclude that the scaling law for the *MAD* (of the middle particle) in a file with a density that is not fixed should follow:

$$< |R| > \sim \frac{1}{n^{\frac{1-a}{1+a}}} < |R| >_{free}. \quad (31)$$

This equation was used for deriving Eq. (7). Indeed, one can use this equation also for files that are not Brownian. Interestingly, this equation shows that the effect of the expansion in not trivial: when the density is not fixed, cooperation has a smaller effect. Although it is still required that *n* particles will cooperate and move in the direction of the propagation, the fact that there is an expansion process towards the periphery, facilitates the demand for cooperation. Since the power $\frac{1-a}{1+a}$ is always smaller than 1 when *a* is smaller than one, the cooperation term $\frac{1}{n^{\frac{1-a}{1+a}}}$ demands that a smaller amount of particles than those that actually exist in the interval will cooperate. The physical reason is very clear: the particles simply move towards the periphery with higher tendency than they move towards the origin, effectively causing a process of file diffusion with a force towards the periphery. Since the scaling law in Eq. (31) holds for the particle in the middle, this force helps the propagation of the tagged one, and it is seen in the form of the cooperation term.

II.c.2. PDFs in Heterogeneous files

The multi-walkers PDF.- Heterogeneous files obey the following equation of motion:

$$\partial_t P(\boldsymbol{x}, t \mid \boldsymbol{x_0}) = \sum_{j=-M}^{M} D_j \partial_{x_j} \partial_{x_j} P(\boldsymbol{x}, t \mid \boldsymbol{x}_0), \quad (32)$$

with the boundary conditions:

$$(D_j \partial_{x_j} P(\boldsymbol{x}, t \mid \boldsymbol{x_0}))_{x_j = x_{j+1}} = (D_{j+1} \partial_{x_{j+1}} P(\boldsymbol{x}, t \mid \boldsymbol{x_0}))_{x_{j+1} = x_j}, \quad (33)$$

where, $j = -M, \ldots, M-1$, and with the initial condition, Eq. (19). We *approximate* the solution of Eqs. (32)-(33) with the expression,

$$P(\boldsymbol{x}, t \mid \boldsymbol{x_0}) \approx \frac{1}{c_N} \sum_p e^{-\sum_{j=-M}^{M} \frac{(x_j - x_{0,j}(p))^2}{4tD_j}}. \quad (34)$$

Equation (34) is our first main result in this part. The proof is presented in what follows.

Proof of equation Eq. (34).- We first show that Eq. (34) reduces to Eq. (19) in the limit, $t \to 0$.

In this limit we find:

$$P(\boldsymbol{x}, t \to 0 \mid \boldsymbol{x_0}) = \sum_p \prod_{j=-M}^{M} \delta(x_j - x_{0,j}(p)), \tag{35}$$

since any normalized Gaussian reduces to a Delta function in the limit $t \to 0$:

$$\left(\frac{1}{\sqrt{4\pi D_j t}} e^{-\frac{(x_j - x_{0,j}(p))^2}{4tD_j}}\right)_{t\to 0} \to \delta(x_j - x_{0,j}(p).$$

Yet, since the solution must always obey Eq. (34), only the ordered permutation survives, say, permutation $p = 1$, obeying:

$$-\infty \le x_{0,-M} \le x_{0,-M+1} \le \cdots \le x_{0,M-1} \le x_{0,M} \le \infty.$$

Namely, we have:

$$P(\boldsymbol{x}, t \to 0 \mid \boldsymbol{x_0}) = \prod_{j=-M}^{M} \delta(x_j - x_{0,j}(1)),$$

and this is indeed the required form of the initial condition.

Next, we show that the PDF in Eq. (34) fulfills the equation of motion. First, we take its time derivative:

$$I = \partial_t \left(\frac{1}{c_N} \sum_p e^{-\sum_{j=-n}^{n} \frac{(x_j - x_{0,j}(p))^2}{4\mathrm{t}D_j}}\right) = \left(\frac{\dot{1}}{c_N}\right) \sum_p e^{-\sum_{j=-M}^{M} \frac{(x_j - x_{0,j}(p))^2}{4tD_j}}$$
$$+ \frac{1}{c_N} \sum_p e^{-\sum_{j=-M}^{M} \frac{(x_j - x_{0,j}(p))^2}{4tD_j}} \left[\frac{1}{t} \sum_{i=-M}^{M} \frac{(x_i - x_{0,i}(p))^2}{4tD_i}\right]. \tag{36}$$

Now, using,

$$\left(\frac{\dot{1}}{c_N}\right) = -\frac{N/2}{t} \frac{1}{\prod_{j=-M}^{M} D_j} \frac{1}{(4\pi t)^{N/2}} = -\frac{N/2}{t} \left(\frac{1}{c_N}\right),$$

we have:

$$I = \frac{1}{c_N} \sum_p e^{-\sum_{j=-M}^{M} \frac{(x_j - x_{0,j}(p))^2}{4tD_j}} \left[\frac{1}{t} \sum_{i=-M}^{M} \left(\frac{(x_i - x_{0,i}(p))^2}{4tD_i} - \frac{1}{2}\right)\right]. \tag{37}$$

Here, we used the relation, $N = 2M + 1$. Now, applying the operator in the right hand side of

Eq. (32) on Eq. (34), we see:

$$II = \frac{1}{c_N}\sum_{i=-M}^{M} D_i \partial_{x_i}\partial_{x_i} \sum_p e^{-\sum_{j=-M}^{M}\frac{(x_j - x_{0,j}(p))^2}{4tD_j}},$$

giving,

$$II = \frac{1}{c_N}\sum_{j=-M}^{M} D_j \partial_{x_j} \sum_p -2\frac{x_j - x_{0,j}(p)}{4tD_j} e^{-\sum_{i=-M}^{M}\frac{\left(x_i - x_{0,i}(p)\right)^2}{4tD_i}}$$

$$= \frac{1}{c_N}\sum_{j=-M}^{M} D_j \sum_p \left(\left(-2\frac{x_j - x_{0,j}(p)}{4tD_j}\right)^2 - \frac{1}{2tD_j}\right) e^{-\sum_{i=-M}^{M}\frac{\left(x_i - x_{0,i}(p)\right)^2}{4tD_i}}.$$

This equation is rewritten in the form of,

$$II = \frac{1}{c_N}\sum_p e^{-\sum_{i=-M}^{M}\frac{\left(x_i - x_{0,i}(p)\right)^2}{4tD_i}} \sum_{j=-M}^{M}\left(\frac{\left(x_j - x_{0,j}(p)\right)^2}{4tD_j} - \frac{1}{2t}\right). \quad (38)$$

Cleary, Eq. (38) and Eq. (37) are equivalent.

Now, for the boundary conditions: applying on the PDF the left hand side of the boundary condition in Eq. (33), we find,

$$L = \left(D_i\,\partial_{x_i}\sum_p e^{-\sum_{j=-M}^{M}\frac{(x_j - x_{0,j}(p))^2}{4tD_j}}\right)_{x_i = x_{i+1}\equiv \mathrm{y}} =$$

$$\frac{-2}{t}\sum_p (y - x_{0,i}(p)) e^{-\left[\frac{(y - x_{0,i}(p))^2}{4tD_i} + \frac{(y - x_{0,i+1}(p))^2}{4tD_{i+1}} + \sum_{j'=-M}^{M}\frac{(x_j - x_{0,j}(p))^2}{4tD_j}\right]} \equiv \sum_p \tilde{L}(p). \quad (39)$$

Here, the exponential's argument counts all the coordinates excluding x_i and x_{i+1}. Applying on the PDF the right hand side of the boundary condition, one sees:

$$R = \left(D_{i+1}\,\partial_{x_{i+1}}\sum_p e^{-\sum_{j=-M}^{M}\frac{(x_j - x_{0,j}(p))^2}{4tD_j}}\right)_{x_i = x_{i+1}\equiv \mathrm{y}} =$$

$$\frac{-2}{t}\sum_p (y - x_{0,i+1}(p)) e^{-\left[\frac{(y - x_{0,i}(p))^2}{4tD_i} + \frac{(y - x_{0,i+1}(p))^2}{4tD_{i+1}} + \sum_{j'=-M}^{M}\frac{(x_j - x_{0,j}(p))^2}{4tD_j}\right]} \equiv \sum_p \tilde{R}(p). \quad (40)$$

Now, we look on permutations $p^{\#}$ and p^{*}: these are the same excluding the values for $x_{0,i}$ and $x_{0,i+1}$. In particular, for permutation $p^{\#}$, we set:

$$p^{\#}: \left\{\{p'\}, x_{0,i}(p^{\#}) = X, x_{0,i+1}(p^{\#}) = Y\right\},$$

and for permutation p^{*}, we set:

$$p^{*}: \left\{\{p'\}, x_{0,i}(p^{*}) = Y, x_{0,i+1}(p^{*}) = X\right\}.$$

The set $\{p'\}$ contains permutations of all the initial coordinates excluding the coordinates $x_{0,i}$ and $x_{0,i+1}$. Now, in what follows we calculate, $\sum_{p}\cdot$ over $p = 1, \dots, N!$ permutations with operations over three variables:

$$\sum_{p} \tilde{R}(p) = \sum_{Y} \sum_{X \neq Y} \sum_{p'} \tilde{R}(p', X, Y), \tag{41.1}$$

and we use the equality,

$$\sum_{Y} \sum_{X \neq Y} \sum_{p'} \tilde{R}(p', X, Y) = \sum_{Y} \sum_{X \neq Y} \sum_{p'} \tilde{R}(p', Y, X). \tag{41.2}$$

(Cleary, the above couple of equations hold also for $\tilde{L}(p)$.) We will show that the following relation holds in the limit $t \to \infty$:

$$\tilde{L}(p^{\#}) + \tilde{L}(p^{*}) \approx \tilde{R}(p^{\#}) + \tilde{R}(p^{*}). \tag{42}$$

Proving Eq. (42) is sufficient for proving that Eq. (34) approximates the boundary conditions (33), since with Eqs. (41)-(42), we have the full boundary condition.

Starting from Eq. (42), we have for the left hand side:

$$\frac{\tilde{L}(p^{\#}) + \tilde{L}(p^{*})}{c} = (y - X) e^{-\left[\frac{(y-X)^2}{4tD_i} + \frac{(y-Y)^2}{4tD_{i+1}}\right]} + (y - Y) e^{-\left[\frac{(y-Y)^2}{4tD_i} + \frac{(y-X)^2}{4tD_{i+1}}\right]}, \tag{43.1}$$

where the right hand side of Eq. (42) reads:

$$\frac{\tilde{R}(p^{\#})+\tilde{R}(p^{*})}{c} = (y-Y)e^{-\left[\frac{(y-X)^2}{4tD_i}+\frac{(y-Y)^2}{4tD_{i+1}}\right]} + (y-X)e^{-\left[\frac{(y-Y)^2}{4tD_i}+\frac{(y-X)^2}{4tD_{i+1}}\right]}. \qquad (43.2)$$

The factor c that appears in Eqs. (43) reads:

$c = \frac{-2}{t}\sum_{p'} e^{-\sum_{j'=-M}^{M}\frac{(x_j - x_{0,j(p')})^2}{4tD_j}}$.

Now, the exponential factor $e^{-\left[\frac{(y-X)^2}{4tD_i}+\frac{(y-Y)^2}{4tD_{i+1}}\right]}$ is one when $t \to \infty$, and Eq. (43.1) is rewritten:

$$\frac{\tilde{L}(p^{\#})+\tilde{L}(p^{*})}{c}\Big|_{t\to\infty} = (y-X)\left(1 - o\left(\frac{(y-X)^2}{4tD_i}+\frac{(y-Y)^2}{4tD_{i+1}}\right)\right) + (y-Y)\left(1 - o\left(\frac{(y-Y)^2}{4tD_i}+\frac{(y-X)^2}{4tD_{i+1}}\right)\right), \qquad (44.1)$$

and similarly, Eq. (43.2) reads:

$$\frac{\tilde{R}(p^{\#})+\tilde{R}(p^{*})}{c}\Big|_{t\to\infty} = (y-Y)\left(1 - o\left(\frac{(y-X)^2}{4tD_i}+\frac{(y-Y)^2}{4tD_{i+1}}\right)\right) + (y-X)\left(1 - o\left(\frac{(y-Y)^2}{4tD_i}+\frac{(y-X)^2}{4tD_{i+1}}\right)\right), \qquad (44.2)$$

Clearly, Eq. (44.1) and Eq. (44.2) are equal in a leading order of $o\left(\frac{1}{t}\right)$, and thus, Eqs. (44) prove Eq. (42), and thus prove Eq. (34).

The tagged-walker PDF.- Using Eq. (34), we approximate the PDF of the tagged particle in the heterogeneous file with,

$$P(r,t \mid r_0) \approx \frac{1}{c_N}\sum_{\tilde{p}} e^{-\sum_{j=-n}^{n}\frac{(r_d - x_{0,j(\tilde{p})})^2}{4tD_j}} \leq \frac{1}{c_N} e^{\frac{-R_d^2}{4\tau}\sum_{j=1}^{n} 1/D_j}. \quad (45)$$

Here, $\tau = \Delta^{-2}\Lambda t$. Equation (45) is based on the same approach that relates Eq. (22) with Eq. (29) for files with the same diffusion coefficient for all the particles. Several additional comments are presented in what follows for explaining this relation.

Comments on the approximation in Eq. (45) for a tagged particle.- Here, we relate Eq. (34) with the PDF of a tagged particle in the file,

$$P(r,t \mid r_0) \approx \frac{1}{c_N}\sum_{\tilde{p}} e^{-\sum_{j=-n}^{n}\frac{(r_d - x_{0,j(\tilde{p})})^2}{4tD_j}}. \quad (46)$$

In Eq. (46), $\tilde{p}$ goes over the relevant permutations (about n^2 permutations); see the discussion in the previous title around Eqs. (27), for further details on the permutations in $\tilde{p}$. We then discuss the technical details that further approximate $P(r,t \mid r_0)$ with,

$$\frac{1}{c_N}\sum_{\tilde{p}} e^{-\sum_{j=-n}^{n}\frac{(r_d - x_{0,j(\tilde{p})})^2}{4tD_j}} \leq \frac{1}{c_N} e^{\frac{-R_d^2}{4\tau}\sum_{j=1}^{n}(\Lambda/D_j)}. \quad (47)$$

In Eqs. (45)-(47), $1/c_N$ is always a normalization constant, and in Eq. (47) $R_d = r_d/\Delta$ (where, $r_d = r - r_0$ is the tagged particle coordinate minus its initial position) and $\tau = \frac{\Lambda}{\Delta^2}t$ are scaled distance (without dimensions) and scaled time (without dimension), respectively. Also, we recall that Δ ($\equiv 1/\rho_0$) is a microscopic length scale and Λ is the fastest diffusion coefficient in the file.

The relation connecting Eqs. (34) and (46), written in a symbolic way, reads,

$$\frac{1}{c_N}\sum_{p} e^{-\sum_{j=-M}^{M}\frac{(x_j - x_{0,j(p)})^2}{4tD_j}} \quad \longmapsto \quad \frac{1}{c_N}\sum_{\tilde{p}} e^{-\sum_{j=-n}^{n}\frac{(r_d - x_{0,j(\tilde{p})})^2}{4tD_j}}. \quad (48)$$

Equation (48) is based on the relation connecting the corresponding quantities in a file with a unique diffusion coefficient; see Eq. (22) and Eq. (27.2). In fact, we can carry on precisely the

same analysis that was used in obtaining Eq. (27.1) from Eq. (22), here, for the heterogeneous file, for deriving Eq. (48). The fact that D_j appears in the denominator of the exponential does not change the number of the particles in the length $\sqrt{\Lambda t}$, and this is the reason that the same analysis holds for both systems.

Now, for explaining the upper bound of, $\sum_{\tilde{p}} e^{-\sum_{j=-n}^{n} \frac{(r_d - x_{0,j}(\tilde{p}))^2}{4tD_j}}$, in Eq. (47), we notice that $x_{0,\pm j}(\tilde{p})$ is always at a distance from r_d that is not smaller than $\sqrt{4tD_j}$. In fact, we should set,

$$x_{0,\pm j}(\tilde{p}) \to \pm \bar{R}, \tag{49}$$

where $\bar{R}$ is a large quantity that is proportional to M. The reason is simple: $x_{0,\pm j}(p)$ should reflect all the M coordinates from the left (right) of r for $x_{0,j}(p)$ [$x_{0,-j}(p)$], and for this we must use an average quantity, say, $\bar{R}$ ($-\bar{R}$), and this quantity is positive (negative) and large (in absolute value) when M is large. See also the discussion above Eq. (27.2).

Using Eq. (49) in the exponentials' arguments in Eq. (47) gives,

$$(r_d - x_{0,\pm j}(\tilde{p}))^2 = r_d^2 \mp 2r_d\bar{R} + \bar{R}^2,$$

and so,

$$\frac{1}{c_N}\sum_{\tilde{p}} e^{-\sum_{j=-n}^{n} \frac{(r_d - x_{0,j}(\tilde{p}))^2}{4tD_j}} \quad \longmapsto \quad \frac{1}{c_N} e^{-\sum_{j=1}^{n} \frac{r_d^2 + \bar{R}^2}{2tD_j}}. \tag{50}$$

Renormalizing Eq. (50) with respect to r_d gives Eq. (47).

Solving the PDF for the heterogeneous walker, Eq. (45).- We proceed from Eq. (45) when calculating $\sum$ in last factor in Eq. (45). These calculations are more complicated than those performed for the simple file. Firstly, for a heterogeneous file that its diffusion coefficients are drawn from Eq. (2), any group of n particles (taken from the N particles in the file) must have the following values for their diffusion coefficients,

$$D_j \approx \Lambda(1 - (j-1)/n)^{1/(1-\gamma)} \qquad ; \qquad 1 \le j \le n,$$

where the values of the diffusion coefficients are ordered from the largest towards the smallest. This relation's accuracy increases as $n \to \infty$. See the discussion in what follows.

Secondly, we need to find $n(t)$. This is found from the equation:

$$\frac{\tilde{r}(n)^2}{\tilde{D_n}} = t. \qquad (51)$$

Relation (51) represents the arguments in all the exponentials in Eq. (45). $\tilde{r}(n)$ is simply found from the density law in the system, $n \approx (\tilde{r}/\Delta)^{1-a}$. The diffusion coefficient $\tilde{D_n}$ appearing in Eq. (51) must represent a bunch of slow particles in the interval that has in it n particles, as these particles affect the result the most. Yet, $\tilde{D_n}$ is a typical slow diffusion coefficient, and not necessarily the slowest. We estimate $\tilde{D_n}$ as, $\tilde{D_n} = \Lambda n^{-\gamma/(1-\gamma)}$. The derivation of this relation is spelled out around Eq. (12). Note that when $\gamma \to 1$, $\tilde{D_n}$ reaches the value of the slowest diffusion coefficient from a group of n particles. Yet, for a relative fast system $\tilde{D_n}$ approaches a constant independent of n. A similar trend in seen in the behavior of the average diffusion coefficient, which vanishes when $\gamma \to 1$ and has a finite value (larger than zero) when $\gamma \to 0$. Now, using the above expressions for $\tilde{r}(n)$ and $\tilde{D_n}$ in Eq. (51), we find,

$$n \approx \tau^{\frac{(1-a)(1-\gamma)}{2-\gamma(1+a)}}. \qquad (52)$$

Eq. (52) for a constant density file and Eq. (14) are equivalent. Now, substituting Eq. (52) in Eq. (45) yields the PDF for the tagged particle in a heterogeneous file:

$$P(r,t \mid r_0) \le \frac{1}{c_N} e^{\frac{-R_d^2}{4\tau}\sum_{j=1}^{n}(1-\frac{j-1}{n})^{\frac{-1}{1-\gamma}}} = \frac{1}{c_N} e^{\frac{-R_d^2}{4\tau} n^{\frac{1}{1-\gamma}}} = \frac{1}{c_N} e^{\frac{-R_d^2}{4\tau}\tau^{\frac{(1-a)}{2-\gamma(1+a)}}}. \qquad (53)$$

A Gaussian PDF is specified through its variance, and so,

$$\langle R_d^2 \rangle = 2\tau^{\frac{1-\gamma}{2c-\gamma}}, \qquad c = 1/(1+a)\ . \qquad (54)$$

Equations (53) and (54), together with Eq. (34), are the most important results of heterogeneous files. Note that Eq. (54) is obtained from Eq. (53), and so it is the upper bound of the MSD of

this file. Yet, we show in scaling law analysis (and in simulations shown in what follows), that this is in fact the asymptotic limit of the actual MSD.

Examining Eq. (54), we note the following. In the limit of, $\to 0$, $\langle R_d^2 \rangle \sim \tau^{(1+a)/2}$. This result and Eq. (7) for a Brownian file are equivalent. We conclude from this result that when there are just few slow particles in the file, the MSD here and in a simple file scale similarly. Thus, this result gives the criteria when $W(D)$ affects the diffusion process significantly. Now, in the limit of a constant density, a=0, we have, $\langle R_d^2 \rangle \approx \tau^{(1-\gamma)/(2-\gamma)}$; a result that was obtained from scaling laws for heterogeneous files with a constant density; see Eq. (15). Note also that when, $\gamma \to 1$, $\langle R_d^2 \rangle \approx 1$, namely, in this limit the system is frozen. Equation (54) also predicts a cancellation of opposing effects: slow diffusion resulting from many slow particles and fast diffusion resulting from a low particles' density can cancel each other; when: $a = \gamma/(2-\gamma)$, a simple file scaling is seen, $\langle R_d^2 \rangle \sim \tau^{1/2}$, yet the actual file is totally heterogeneous.

Finally, we note here that a very different result for the MSD than Eq. (54) is obtained in a heterogeneous file obeying Eq. (2), when all the particles start at the origin; see Ref. [2.21] for a discussion regarding such a variant.

The form of D_j.- Here, we calculate the form of D_j appearing just above Eq. (51).

Given the PDF,

$$W(D) = (1-\gamma)\Lambda^{-1}(D/\Lambda)^{-\gamma} \quad ; \quad 0 \le \gamma < 1,$$

defined in the interval, $0 \le D \le \Lambda$, we draw n random numbers from this PDF. What is the shape of the curve when we plot these random numbers when ordering them from the largest value towards the smallest? Answering this question gives,

$$D_j \approx \Lambda(1-(j-1)/n)^{1/(1-\gamma)}. \quad (55)$$

This expression's accuracy increases with the value of n.

For proving Eq. (55), we first write the expression for drawing a random diffusion coefficient from $W(D)$ using the unit density,

$$W_u(x) = 1 \quad ; \quad 0 \le x \le 1.$$

We use the relation,

$$W(D)dD = W_u(x)dx,$$

and find,

$$D = \Lambda {x_r}^{1/(1-\gamma)}. \quad (56)$$

In Eq. (56), x_r is a random number drawn from the unit PDF, $W_u(x)$. When there are n random numbers, $\vec{x}_r$ is a vector of length n. For proceeding, we look for the functional form of element *j* in this vector after ordering it from the largest value to the smallest. We call this vector ($\vec{x}_r$ with ordered elements), $\vec{y}_r$. It is clear that the largest value of $\vec{y}_r$ is one; the smallest value is $1/n$ (this is shown in what follows). As the density $W_u(x)$ is fixed, $\vec{y}_r$ must have the form,

$$\vec{y}_r = 1, 1-\tfrac{1}{n}, 1-\tfrac{2}{n}, \dots, 1-\tfrac{n-1}{n}. \quad (57)$$

Equation (57) proves Eq. (55).

For showing that the smallest value in $\vec{y}_r$ is $1/n$, we calculate the PDF of the smallest number from possible $n+1$ random numbers drawn independently from $W_u(x)$:

$$\widetilde{W_u}(x; n+1) = W_u(x)\left(\int_x^1 W_u(y)dy\right)^n \approx W_u(x)e^{-nx}. \quad (58)$$

Similar with the analysis of extreme value statistics in scaling laws calculations [around Eqs. (9-10)], we find the typical value of the smallest number drawn from $\widetilde{W_u}(x; n+1)$, $x_{t.s.}$, when first demanding that e^{-nx} is not smaller than e^{-1}; namely:

$x^* \lesssim 1/n.$

Using this upper bound in the re-normalized PDF in Eq. (58) gives:

$$\widetilde{W_u}(x^*; n+1) = n. \qquad (59)$$

Finally, the typical smallest value of the vector $\vec{y}_r$, $x_{t.s.}$, is the inverse of $\widetilde{W_u}(x^*; n+1)$ in Eq. (59), that is,

$x_{t.s.} = 1/n.$

It is very simple seeing that this analysis is very accurate even for 501 particles (the number of particles used in our simulations) in simulations. Results from several simulations (for three different values of γ) are shown in Fig. II.3. Coincidence of the simulations with the formula in Eq. (55) is evident.

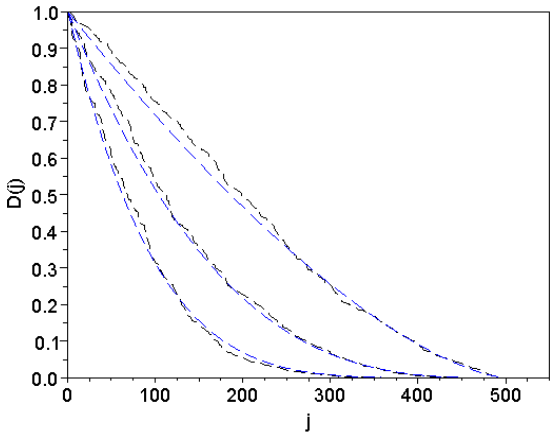

Fig II.3 Results from simulations drawing 501 diffusion coefficients from Eq. (2), and ordering them from the largest to the smallest; curves are obtained for 3 different values of γ, $\gamma = \frac{1}{3}, \frac{2}{3}, \frac{2.429}{3}$. The curve with the smaller value of γ is to the right of those with lager values of γ. Here, $\Lambda = 1$. This figure also shows the curves from Eq. (55) for each value of γ. Coincidence among the curves from the simulations and the estimated curves is evident.

II.d. Simulations of normal files

We perform *off*-lattice simulations of Eq. (32) with reflecting interactions between point particles. The fact that the particles are point-like is indeed shown in the equation of motion, yet, does not change the long time statistics of the file compared with results of files on lattices. This is simply shown in simulations. (In fact, simulations are always lattice-like since the smallest length scale is limited with the precision of the machine.) In the simulations, each particle is assigned a diffusion coefficient from the PDF in Eq. (2) (Λ=1 in the simulation). (We use units without dimensions all over). The j^{th} particle is positioned at, $x_{0,j}$=sign(j)$|j|^{1/(1-a)}\Delta$ (Δ=1.3 in the simulation). We set *N=501* particles. In each time step (*dt* = 0.13 in the simulations), each particle is moved relative to its position according to the equation,

$dx_j = 2(q - 1/2)\sqrt{2D_j t}$,

where q is a random number from the unit PDF, and is chosen for each particle at each time step. The particles' locations are ordered after each time step. The interval's length is bound: edges particles can't move further than their initial conditions plus a room for several full jumps in the direction that extends the initial interval length. The above iteration scheme is executed over and over and over again (three millions time steps are performed for each simulation). Note that in the above simulations' rules, the boundary conditions are *always* fulfilled. Also, note that the above simulations' rules were also used for simple files; e.g. files with the same diffusion coefficient. Yet, these rules hold also for the heterogeneous file. Here, the reflection principle (that is, the ordering of the particles after each cycle of jumps) represents: (a) elastic collisions among particles that can clearly also represent particles with distribution of diffusion

coefficients, and (b) Brownian dynamics, so the particles momenta decay after each jump relatively fast, and so in the next cycle of jumps, the particles do not drag previous velocities.

We perform extensive simulations. Each simulation has different values for a and γ where, $a=0,\ 1/3,\ 2/3,$ and, γ=0, 1/3, 1/2, 2/3. In each simulation, we calculate the *MSD* for thirty particles from the file. For each simulation (defined with a specific values for γ and a), the run time for the simulation and the *MSD*-calculations is three minutes on a standard 3.37 GHz PC.

Figure II.4 presents the results for the *MSD* from all the simulations. Each panel shows *MSD*-curves for three values of a each with the same value of γ. The analytical curves obtained from Eq. (54) are also shown. The curves coincide with the numerical results in a satisfactory level. The only point to note is that as a increases, converges occurs at larger times. This is an expected behavior for a file with particle's density that is not fixed.

In light of the simulations' results, a final remark is made on the interpretation of the limit of long times. In this part, we used this limit in deriving the statistics of the heterogeneous file. Indeed, several interpretations for this limit were given. Yet, we can use Fig. II.4 for further define the meaning of long times. Figure II.4 shows that this limit depends on the value of γ and a: when γ and/or a are large, the coincidence of the simulations' curves and the curves obtained from Eq. (54) happens at relatively larger times; plus, at smaller times, the difference among the curves is, in most cases, larger when γ and a are larger. So, we say that a long time limit corresponds to the time, t^*, it takes a particle to reach a distance r^* from its origin that has n^* particles in it. t^* is then estimated with Eq. (18): $r^* \sim \Delta {n^*}^{1/(1-a)} \sim \Delta\sqrt{\langle R_a^2 \rangle}$. These relations give: $t^* \sim \sim \frac{\Delta^2}{\Lambda} {n^*}^{2/[\mu(1-a)]}$, where μ is the scaling power in Eq. (54). We use $n^* = 35$ as a safe-bound for t^*, as the value of 35 (events) is considered a large number in statistics. From Fig. 1, it is

clear that also for $n^* \approx 9$ the coincidence among the simulations' results and the curves obtained from Eq. (54) is excellent.

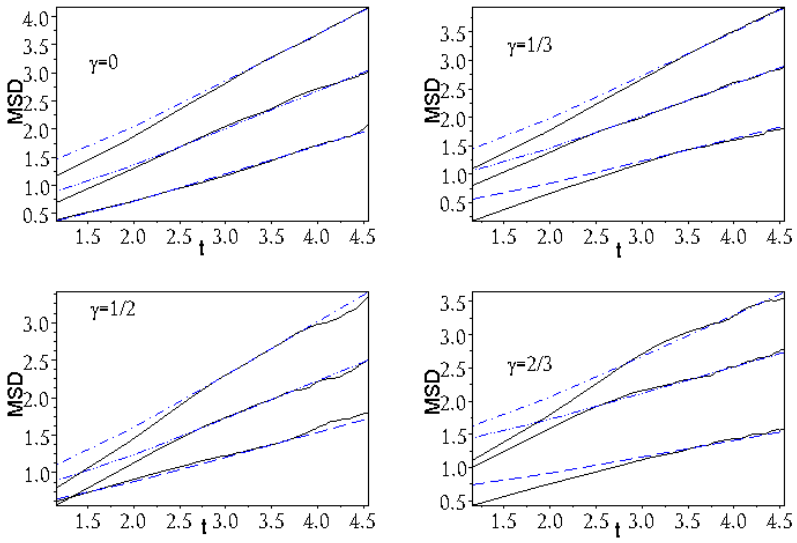

Fig II.4 (color online) The *MSD* on a log-log scale from twelve different simulations. Each simulation has specific values for *a* and γ, where: *γ*=0, 1/3, 1/2, 2/3, and *a*=0, 1/3, 2/3. Each panel has a constant value of γ (the smallest value of γ is in the top-right panel and γ increases in a z-like shape). Each curve (in a given panel) corresponds to a different value of *a*, where a lower curve always has a smaller value of *a*. The analytical curves from Eq. (54) are also shown, and coincide nicely with the results from the simulations. [The free parameter of any analytical curve is always chosen to coincide best with the curve of the simulation. Yet, the curve's slope is obtained from Eq. (54).] Note that the *x*-axis in the figure is obtained when monitoring the value of t_j every, 10^{Aj} time units (A is a number), and then taking the log of the time vector. The Y axis is the log of the monitored *MSD*.

II.e. Concluding remarks

In this chapter, chapter **II**, we dealt with normal stochastic dynamics of heterogeneous hard spheres in a very long strait: heterogeneous walkers in a channel. Each walker has a diffusion coefficient drawn randomly from a PDF, $W(D) \sim (D/\Lambda)^{-\gamma}$, $0 \leq \gamma < 1$, for small *D*. The initial positions are also distributed such that the initial particles' density law obeys, $\rho(l) \sim \rho_0 (l/\Delta)^{-a}$, $0 \leq a \leq 1$, where l is the distance from the orgin. We first derive the approximation for the

multi-walkers PDF for heterogeneous files: $P(\boldsymbol{x},t \mid \boldsymbol{x_0}) \approx \frac{1}{c_N}\sum_p \exp\left(\frac{-1}{4t}\sum_{j=-M}^{M}\frac{(x_j - x_{0,j}(p))^2}{D_j}\right)$. From this PDF, we derive the statistics of the tagged particle in heterogeneous files: $\langle R_d^2\rangle = 2\tau^{\frac{1-\gamma}{2c-\gamma}}$, $c = 1/(1+a)$, and, $P(r,t \mid r_0) \sim \frac{1}{c_N} e^{\frac{-R_d^2}{2<R_d^2>}}$. The same results for the tagged particle's *MSD* were obtained using additional two approaches: scaling law analysis and numerical simulations. We also obtained results for deterministic files with a constant particles' density and distribution in velocities of the form of Eq. (2); here, using scaling law analysis, we found that the *MAD* obeys: $\langle |R_d| \rangle \sim \tau^{\frac{1-\gamma}{2-\gamma}}$. All the above results are valuable for files in which the walkers are not identical, and differ in, for example, mass, size, or composition, and in the context of biological channels.

Still, there is an interesting generalization of the above: anomalous files. In an anomalous file, the basic dynamics are such that the jumping time PDF (for individual jumps) decays like a power-law. (A jumping time PDF in a Brownian file decays exponentially.) Anomalous files exhibit a rich spectrum of behaviors, where the nature of the anomaly of the file determines its statistical behavior. Renewal-anomalous files, in which all the particles attempt jumping at the same time, are different than anomalous files that are not renewal, where each particle has its own clock of jumping times [1.14]. Also, anomalous renewal files with fluctuating diffusion coefficients may lead to interesting phenomena; this statement relied on a corresponding system of a free particle presented in Chapter **I**: when a free stochastic particle performs anomalous dynamics and its diffusion coefficient is drawn every jump from a distribution, a transition in the rule for the power that governs the effective waiting-time PDF of the dynamics is seen [1.17]. Anomalous files are presented in the next chapter.

III. Anomalous files: renewal ones and independent ones

III.1. Renewal-anomalous-heterogeneous files

III.1.a. Introduction for renewal files

In the previous chapter, we studied mainly files with normal dynamics. Indeed, the scaling laws enable us obtaining the *MSD* in files that have different basic dynamics; for example, Eq. (II.7) shows:

$$< r^2 > \sim \rho_0^{a-1} < r^2 >_{free}^{(1+a)/2}, \qquad (1)$$

for files with density law obeying Eq. (II.1). Eq. (1) is the MSD also for Newtonian files and renewal-anomalous files. Particles in Newtonian files exchange momentum upon collisions, and have $< r^2 >_{free} \sim t^2$, where in anomalous files, the jumping times for individual jumps are taken from the PDF, $\psi_\alpha(t) \sim\sim t^{-1-\alpha}$ with $0 < \alpha \leq 1$, and have, $< r^2 >_{free} \sim t^\alpha$. In fact, Eq. (1) is correct for renewal files (and for the middle particle when the density is not fixed). Renewal files versus files that are independent are discussed in this chapter, since this difference is important when the dynamics are anomalous.

In this chapter, we study anomalous files from many angels. Indeed, we clarify the distinction among renewal-anomalous files and anomalous files of independent particles, while showing the different behaviors in these files. In a renewal-anomalous file, all particles attempt jumping *at same time*, after residing in their positions for exactly the same period of time. This random period is drawn independently each jump from $\psi_\alpha(t)$. This is a renewal file: there is only one

clock in the system, and each trajectory of a given particle is a renewal process in the sense that the jumping periods are independent random variables. In anomalous files of independent particles, each particle has its own anomalous clock. This difference is the origin for different dynamical behavior; for example, Eq. (1) cannot be used for anomalous files of independent particles, and the *MSD* in such files obeys: $MSD \sim ln^2\ (t)$. The results in this chapter are based on our papers in this subject from 2010-2011 [1.14, 3.1].

In this part of the chapter, we prove analytically that the *MSD* for renewal-anomalous-heterogeneous files scales as the *MSD* of the corresponding Brownian files in the power of α:

$$< r^2 > \sim < r^2 >_{nrml}^{\alpha}, \qquad (2)$$

where $< r^2 >_{nrml}$ appears in Eq. (II.54). Equation (2) is an outcome of a general relation connecting PDFs of Brownian files and renewal-anomalous files; this relation, Eq. (2), is proved here for the first time. Equation (2) generalizes our previous results for renewal files, e.g. Eq. (II.7) (Eq. (1) above), where the file's *MSD* is related with the free particle's *MSD* of the *same dynamics*. Now, we also show here that Eq. (2) can be obtained using scaling law analysis, where such an analysis further explains the relation among Brownian files and renewal-anomalous files. Simulations help supporting the analysis. Further discussion about the applications of renewal-anomalous-heterogeneous files concludes this part of the chapter.

The definition of renewal files.- A very clear way to define the physical model of renewal-anomalous files uses a simulation scheme. We suggest the following scheme: * a random waiting time τ is drawn independently from $\psi_{\alpha}(t)$, * all the particles in the file stand still for this random

period, * after residing in their positions for a time period τ, all the particles try jumping according to the standard rules of the file. * This procedure is carried on over and over and over again.

III.a.2. PDFs, MSD & numerical simulations

Analytical calculations.- We start when writing down the equation of motion for the multi-walkers PDF of the file. This equation is obtained from the equation of motion for a Brownian file when applying a simple convolution on it. Recall that the equation of motion for a Brownian-heterogeneous file reads [see Eq. (II.32)],

$$\partial_t P_{nrml}(\boldsymbol{x}, t \mid \boldsymbol{x}_0) = \sum_{j=-M}^{M} D_j \partial_{x_j} \partial_{x_j} P_{nrml}(\boldsymbol{x}, t \mid \boldsymbol{x}_0) \equiv L_\mu P_{nrml}(\boldsymbol{x}, t \mid \boldsymbol{x}_0). \qquad (3)$$

Here, $P_{nrml}(\boldsymbol{x}, t \mid \boldsymbol{x}_0)$ is the normal dynamics PDF for the file's particles, located at positions $\boldsymbol{x}$, $\boldsymbol{x} = (x_{-M}, x_{-M-1}, \ldots, x_M)$ at time t, starting from an initial condition $\boldsymbol{x}_0$ at time, $t_0 = 0$. Equation (3) is solved with the appropriate boundary conditions, Eq. (II.33), and with the appropriate *initial* condition, Eq. (II.19). The equations for the PDF in a renewal-anomalous-heterogeneous file are obtained from the corresponding Brownian equations (equation of motion and the boundary conditions) when convoluting them with a kernel $k_\alpha(t)$ [where the initial condition is obtained from Eq. (II.19)]. The particular form of the equation of motion reads:

$$\partial_t P(\boldsymbol{x}, t \mid \boldsymbol{x}_0) = \sum_{j=-M}^{M} D_j \partial_{x_j} \partial_{x_j} \int_0^t k_\alpha(t-u)\, P(\boldsymbol{x}, u \mid \boldsymbol{x}_0) du. \qquad (4)$$

The kernel $k_\alpha(t)$ in Eq. (4) is related with the WT-PDF $\psi_\alpha(t)$ of the same renewal dynamics; this relation is made in Laplace space (e.g. [1.7, 1.9]):

$\bar{k}_\alpha(s) = \frac{s\bar{\psi}_\alpha(s)}{1-\bar{\psi}_\alpha(s)}$,

where the Laplace transform of a function $f(t)$ reads, $\bar{f}(s) = \int_0^\infty f(t)\, e^{-st} dt$.

We note that Eq. (4), for a uniform file ($D_j = D$), was introduced in Ref. [3.2]. Yet, we emphasize here that Eq. (4) holds *only* for renewal-anomalous files; that is, for files in which all the particles attempt jumping together. This is the reason that Eq. (4) has a form of a simple convolution. An anomalous file of independent walkers, in which each walker has its own jumping-clock, should have a different equation of motion [see Eq. (12)], leading to a different dynamical behavior than that of renewal-anomalous files. We show this in the next part of this chapter.

Now, we continue with the analysis of renewal-anomalous files, Eq. (4), and write the PDF for the system in terms of the PDF that solves the un-convoluted equation, Eq. (3). The relation is made in Laplace space:

$$\bar{P}(\boldsymbol{x}, s \mid \boldsymbol{x}_0) = \frac{1}{\bar{k}_\alpha(s)} \bar{P}_{nrml}\left(\boldsymbol{x}, s/\bar{k}_\alpha(s) \mid \boldsymbol{x}_0\right). \quad (5)$$

Equation (5) is a central result in renewal-anomalous-files: it relates renewal-anomalous files and the corresponding Brownian files. For proving Eq. (5), we formally solve Eq. (4) in Laplace space:

$$\bar{P}(\boldsymbol{x}, s \mid \boldsymbol{x}_0) = \left(s + \bar{k}_\alpha(s) L_\mu\right)^{-1} P_{nrml}(\boldsymbol{x}, 0 \mid \boldsymbol{x}_0) = \frac{1}{\bar{k}_\alpha(s)} \left(\frac{s}{\bar{k}_\alpha(s)} + L_\mu\right)^{-1} P_{nrml}(\boldsymbol{x}, 0 \mid \boldsymbol{x}_0), \quad (6)$$

and notice that Eq. (3) has a Laplace space solution of the form,

$$\bar{P}_{nrml}(\boldsymbol{x}, s \mid \boldsymbol{x}_0) = \left(s + L_\mu\right)^{-1} P_{nrml}(\boldsymbol{x}, 0 \mid \boldsymbol{x}_0).$$

When using this equation in rewriting the last expression in Eq. (6), we obtain Eq. (5).

The MSD.- From Eq. (5), it is straightforward relating the MSD of normal heterogeneous files and renewal-anomalous heterogeneous files,

$$< \bar{r}^2(s) >= \frac{1}{\bar{k}_\alpha(s)} < \bar{r}^2(s/\bar{k}_\alpha(s)) >_{nrml}. \quad (7)$$

Now, from Eq. (54) we have, $< r^2(t) >_{nrml} \sim t^\mu$, $\mu = \frac{1-\gamma}{2/(1+a)-\gamma}$, and in Laplace space, $< \bar{r}^2(s) >_{nrml} \sim s^{-1-\mu}$, and so Eq. (7) gives,

$< \bar{r}^2(s) >= \frac{1}{\bar{k}_\alpha(s)} (s/\bar{k}_\alpha(s))^{-1-\mu}$.

Using the asymptotic form of $\bar{\psi}_\alpha(s)$ (small s), $\bar{\psi}_\alpha(s) \sim 1-(sT)^\alpha$, we find the kernel in Laplace space, $\bar{k}_\alpha(s) \sim (sT)^{1-\alpha}$, and $< \bar{r}^2(s) >$ follows,

$< \bar{r}^2(s) > \sim \frac{s^{-\alpha(1+\mu)}}{s^{1-\alpha}} = s^{-1-\alpha\mu}$.

This equation reads in time-space,

$$< r^2(t) > \sim t^{\alpha\mu}. \quad (8)$$

The above expression for the *MSD* of a renewal-anomalous file has a very appealing consequence: one can use the results of a file with normal dynamics in the power of α for obtaining the results for the corresponding renewal-anomalous file,

$$< r^2(t) > \sim < r^2(t) >^\alpha_{nrml}. \quad (9)$$

Equations (8) - (9) are among the main results of this paper. Equations (8) - (9) originated from a general relation connecting PDFs of renewal-anomalous files and Brownian files, Eq. (5). In the next paragraph, the same results are derived using scaling law analysis. This unravels another interesting relation connecting renewal-anomalous files and Brownian files.

Scaling law analysis.- In this paragraph, we derive a similar relation to Eq. (8) in a way that gives additional insights into the behavior of renewal-anomalous files. First, we realize that a Brownian file is a renewal file in which all the particles attempt a jump every time step dt. This is simply seen when simulating the discrete-time-version of the equation of motion, Eq. (4). A consequence of this property is that the average number of attempts for jumping as a function of the time, $< J(t) >$, scales, for any particle in the heterogeneous-Brownian-file, as, $< J(t) > \sim t$. This is found from the general relation for $< \bar{J}(s) >$ for a renewal process with a JT-PDF $\psi(t)$, e.g. [1.7],

$< \bar{J}(s) >= \frac{\bar{\psi}(s)}{s(1-\bar{\psi}(s))}$,

when using the fact that $\psi(t)$ is exponential for a Brownian file. Now, when using this relation for $\psi_\alpha(t)$, we find that for a renewal-anomalous file, $< J(t) > \sim t^\alpha$. The above is used in the following way. First, we recall that for any renewal dynamics, $< r^2(t) >_{free} \sim < J(t) >$, e.g. [1.7], and use this in Eq. (II.7) for writing,

$< r^2(t) > \sim < J(t) >^{(1+a)/2}$.

The next step uses the above also in Eq. (II.54),

$$< r^2(t) > \sim < J(t) >^{\mu} \quad ; \quad \mu = \frac{1-\gamma}{2/(1+a)-\gamma}. \qquad (10)$$

Taking this relation to hold for any renewal process, it is the same as Eq. (8), and is complementary with Eq. (9), and simply generalizes Eq. (II.7) for any renewal stochastic dynamics (since Eq. (II.7) holds for normal dynamics).

There is another way for using $< J(t) >$ in relating a Brownian file with a renewal-anomalous file. Here, we take the trajectory that changes its value every time step dt, and stretch

each time step dt to a random period drawn from the JT-PDF, $\psi_\alpha(t)$. Clearly, this manipulation takes a trajectory with, $< J(t) > \sim t$, and makes it a trajectory with, $< J(t) > \sim t^\alpha$. This suggests using the transformation $t \to t^\alpha$ in $< r^2(t) >_{nrml}$ for obtaining $< r^2(t) >$; namely:

$$< r^2(t) > \sim < r^2(t^\alpha) >_{nrml}. \qquad (11)$$

We will use the above manipulation in the numerical simulations presented in the next paragraph.

Numerical simulations.- Based on the above scheme for simulating renewal-anomalous files, we present in this paragraph the results from extensive simulations. First, Fig. 1 shows a pair of trajectories: the left trajectory is obtained from a simulation of Eq. (3) with $a = 1/3$ and $\gamma = 0$, and the right trajectory is obtained from the left trajectory when applying the manipulation described in area of Eqs. (10)-(11), with $\alpha = 1/3$. Note that the right trajectory is stretched one hundred thousand times when applying the timescale manipulation, forming the whole left trajectory.

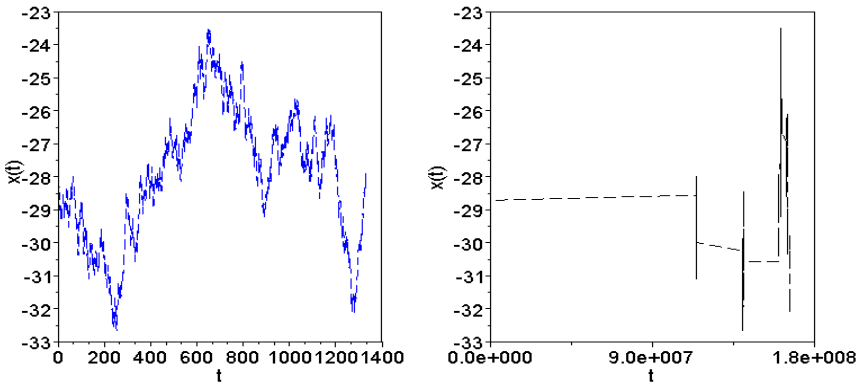

Fig 1 Trajectories from file dynamics. The left trajectory is obtained from a simulation of Eq. (3), with, $D_j \to D$. The right trajectory is obtained from the left trajectory when applying the time-scale manipulation described in paragraph ***scaling law analysis***, with, $\alpha = 1/3$ and $k = 1$. In the simulation, $N = 501$, $dt = 0.13$, $\Delta = 1$, $D = 1$ and $a = 1/3$, where we use units without dimension all over.

Now, for each renewal-anomalous trajectory, such as the right trajectory in Fig.1, we calculate the *MSD*. The results for the *MSD* for renewal-anomalous files are shown in the four panels of Fig. 2. Note that the calculations of the *MSD* from renewal-anomalous trajectories demand taking into account the fact that the original time vector has random increments. The most efficient way to calculate the MSD for such a form of the time vector creates, for each value of t in $< r^2(t) >$, a trajectory that is monitored in time interval of length t, and from this trajectory calculates the value of $< r^2(t) >$.

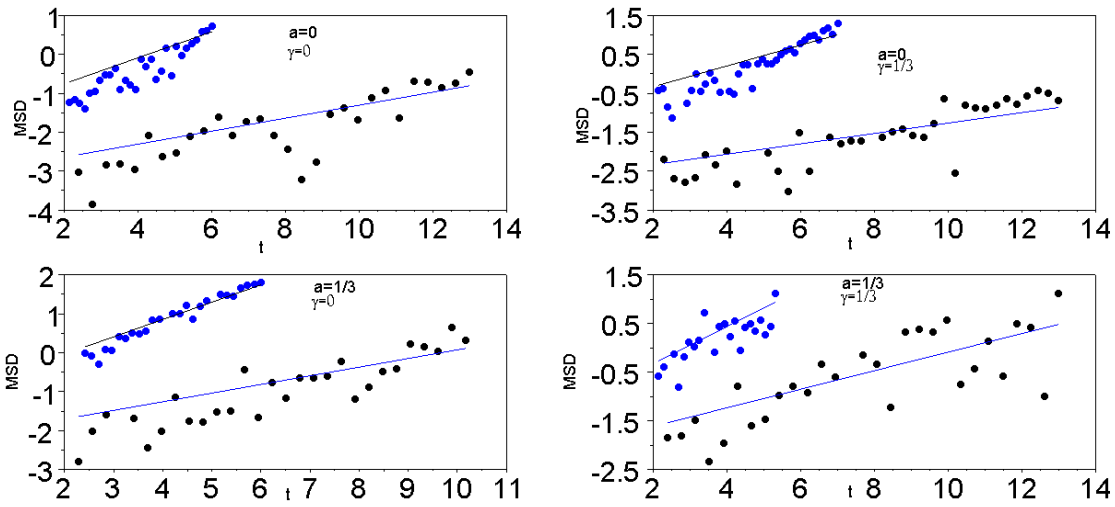

Fig 2 The MSD, on a log-log scale, from extensive simulations for the various values of a, γ and α. Each panel has distinct values of a and γ, written explicitly on the panel, yet the value of α varies, $\alpha = \frac{1}{3}, \frac{2}{3}$. The lower curve in each panel corresponds to $\alpha = 1/3$. The curves from our estimation for the MSD are also presented. The coincidence with the results from the simulations is pretty clear in all cases.

Each panel in Fig. 2 has a constant value of a and γ, taken from the following values: $a = 0, \frac{1}{3}$, and, $\gamma = 0, \frac{1}{3}$, and shows two curves of the *MSD* for the various values of α, $\alpha = \frac{1}{3}, \frac{2}{3}$, where $\alpha = \frac{1}{3}$ for the lower curve. Also shown are the analytical curves from Eq. (8). The curves from the

simulations coincide nicely with the analytical curves. Note that the results for the *MSD* with $\alpha = \frac{1}{3}$ span twelve orders of magnitude.

III.a.3. Applicability of renewal anomalous files

In this part of the chapter, we have showed that the dynamics of walkers in anomalous-renewal files simply scale with the dynamics in heterogeneous files of normal walkers. What are the possible applications of renewal-anomalous-heterogeneous files? The model of renewal-anomalous files can be related pretty naturally with many systems that are possible applications of file dynamics. We present here a particular example, and this is the dynamics of particles in fluctuating pores. Possible realizations of such files include:

- Pores under on-off fields or under temperature changes (say, controlled externally), sensing devices (as was suggested for zeolites, e.g. [3.3]) under on-off fields,
- Channels as sequencing devices (e.g. [3.4]) under on-off fields.

The model relevant for such a fluctuating channel contains a channel that occupies one of two possible states: (1) a state that enables motion, and (2) a state that does not enable motion of particles in it. When the channel occupies the later state, the particles can easily bind the channel. The dynamics of the complex process consist of the following stages:

- The particles diffuse in a channel since the channel is in a mode that enables motion.
- At random times, the channel switches modes. In a switch, a diffusive mode switches for a mode that facilitates the binding of particles to the channel. In this mode of the channel, all the particles bind to the channel very quickly.

- The particles disassociate from the channel at random times, yet simultaneously, as this depends on the time that the channel changes its mode, now, for a mode that enables motion.

The above three stages form the model of the diffusion in a fluctuating channel. Now, in particular cases, the stochastic binding times may indeed be distributed according to a PDF of the form of $\psi_\alpha(t)$: $\psi_\alpha(t)\sim t^{-1-\alpha}$. Recall that we have rationalize the synchronized disassociation of the particles from the pore as a result of large scale fluctuations in the channel shape; yet, the reason for a power-law JT-PDF may be attributed to the interactions of the channel with a heterogeneous medium. It is known that the influence of a heterogeneous medium on a diffusion object can lead to a power-law JT-PDF of the form of $\psi_\alpha(t)$ for the diffusing object, e.g. [1.17]. (In fact, this was discussed in chapter 1.) Now, it is well-known that bio-channels in physiological conditions change their structure constantly, e.g. [1.15], and are in contact with a membrane that is heterogeneous in composition. Thus, renewal-anomalous files may indeed serve as a promising choice for modeling biological pores in not so few cases.

III.b. Anomalous Files of independent walkers

III.b.1. Introduction for anomalous files of independent walkers

In the previous part of this chapter, files that are anomalous and renewal were studied. In such files, the jumping times of the particles are taken from, $\psi_\alpha(t)\sim t^{-1-\alpha}$, $0<\alpha<1$, were all the particles attempt a jump together. In renewal-anomalous files, the MSD scales as the MSD of the corresponding Brownian file in the power of α. In this part of the chapter, we study anomalous files made of independent particles. In such files, a random anomalous time is independently assigned for each particle. The fastest particle attempts a jump, and then, all the random times are adjusted. Finally, the particle that attempted jumping receives a new random time. This system has *N* independent anomalous clocks, where a renewal-anomalous file has only one clock. This is the origin for very different dynamical behaviors: since the clocks are anomalous and independent, the particles are further connected in space, causing further slowness, even relative with renewal-anomalous files. Mathematically, the reason is that at large times, the order of the jumps that enables motion is exponentially small (with the number of particles that are suppose moving), and the jumping times are without a typical timescale (that is, the typical timescale is infinite). The basic manifestation of this is a logarithmic scaling with the time of the MSD per particle, $MSD\sim ln^2\,(t)$. Moreover, and even more exciting, we find a unique phenomenon in such files*:* the formation of clusters. We characterize the criticality of this phase transition showing that the number of particles in clusters at steady state follows, $\sqrt{1-\alpha^3}$. We also prove in many numerical tests that this phenomenon is indeed stable. Finally, we also suggest a link of this phenomenon with the mysterious phenomenon of rafts in membranes [3.5], and with regulation of biological channels [3.6].

Simple numerical exemplification of anomalous independent walkers.- We start with a simple numerical example. In the left panel of Fig. 3, a trajectory from a simulation of anomalous independent walkers is shown in blue (upper curve in this panel). For making a comparison explicit, a trajectory from a *corresponding* renewal-anomalous file is also plotted (lower curve, black). The two trajectories are plotted as a function of the event index, namely, not versus the actual time. Clearly, this panel shows that only the trajectory of anomalous independent walkers exhibits anomalous patterns when plotted as a function of its indices. Importantly, the time vectors of files of anomalous independent walkers and files of renewal-anomalous walkers evolve in a similar way; this is shown in the right panel in Fig. 3 that plots these time vectors as a function of their indices. Basically, this figure shows that anomalous files with independent walkers are much slower than their renewal counterparts.

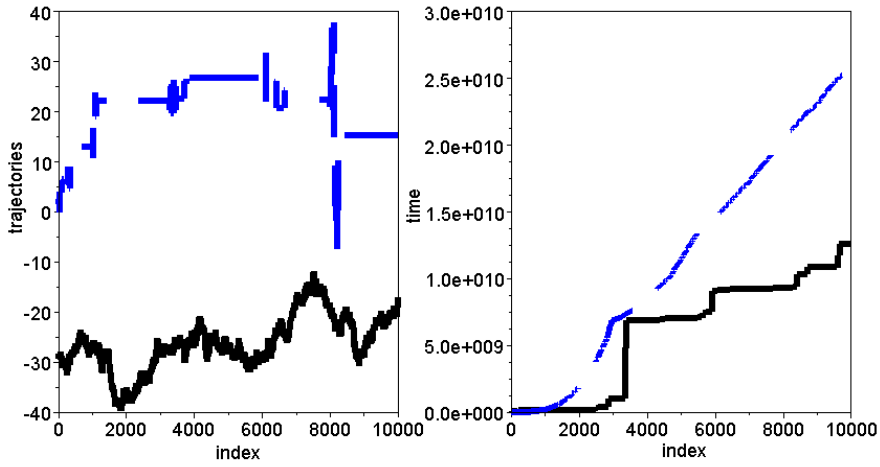

Fig 3 Trajectories from an anomalous file of independent walkers (blue online, upper curve) and a renewal-anomalous-file (black online, lower curve), as a function of the event index, are shown on the left panel. For both trajectories, $\alpha = 1/3$, $\gamma = 0$ and $\alpha = \frac{1}{3}$ (the other file's information is as in Fig. 1). Clearly, the anomalous trajectory of independent walkers shows anomalous patterns and not its renewal counterpart, when plotted versus its indices. The time vectors of both trajectories are of the same magnitude anywhere (right panel). In this right panel the lower curve corresponds to the time vector of the renewal-anomalous file.

Equation of motion for anomalous files of independent particles.- When each particle in the anomalous file is assigned with its own jumping time drawn form $\psi_\alpha(t)$ ($\psi_\alpha(t)$ is the same for all the particles), the anomalous file is not a renewal file. The basic dynamical cycle in such a file consists of the following steps: a particle with the fastest waiting time in the file, say, t_i for particle i, attempts a jump. Then, the waiting times for all the other particles are adjusted: we subtract t_i from each of them. Finally, a new waiting time is drawn for particle i. The most crucial difference among renewal anomalous files and anomalous files that are not renewal is that when each particle has its own clock, the particles are in fact connected also in the time domain, and the outcome is further slowness in the system (proved in what follows). The equation of motion for the PDF $P(\boldsymbol{x},\boldsymbol{t}\mid\boldsymbol{x}_0)$ in anomalous files of independent particles reads:

$$\partial_{t_i}P(\boldsymbol{x},\boldsymbol{t}\mid\boldsymbol{x}_0)=D_i\partial_{x_i}\partial_{x_i}\int_0^{t_i}k_\alpha(t_i-u_i)\,P(\boldsymbol{x},\boldsymbol{t}'^{(i)},u_i\mid\boldsymbol{x}_0)du_i \quad ; \quad -M\le i\le M. \qquad (12)$$

Note that the time argument in the PDF $P(\boldsymbol{x},\boldsymbol{t}\mid\boldsymbol{x}_0)$ is a vector of times: $\boldsymbol{t}=\{t_i\}_{i=-M}^{M}$, and $\boldsymbol{t}'^{(i)}=\{t_c\}_{c=-M,c\neq i}^{M}$. Adding all the coordinates and performing the integration in the order of faster times first (the order is determined randomly from a uniform distribution in the space of configurations) gives the full equation of motion in anomalous files of independent particles (averaging of the equation over all configurations is therefore further required). Indeed, even Eq. (12) is very complicated, and averaging further complicates things. This is the reason that we derive scaling-laws and apply numerical simulations for solving anomalous files of independent particles. The main result is that such files form clusters of particles for anomalous α that pretty much stay in the spot for long times. This phenomenon of a phase transition depending on α is

unique, namely, it doesn't occur in other types of files, and is reflected in the form of the equation of motion.

III.b.2. The MSD & Numerical results

Scaling law for anomalous files of independent particles.- Here, we study anomalous files of independent particles using scaling laws. Firstly, we write down the scaling law for the mean absolute displacement (*MAD*) in a renewal file with a constant density [1.12-1.14]:

$$< |r| > \sim < |r| >_{free}/n. \qquad (13)$$

Here, n is the number of particles in the covered-length $< |r| >$, and $< |r| >_{free}$ is the *MAD* of a free anomalous particle, $< |r| >_{free} \sim t^{\alpha/2}$. In Eq. (13), n enters the calculations since all the particles within the distance $< |r| >$ from the tagged one must move in the same direction in order that the tagged particle will reach a distance $< |r| >$ from its initial position. Based on Eq. (13), we write a generalized scaling law for anomalous files of independent particles:

$$< |r| > \sim \frac{<|r|>_{free}}{n} f(n) \quad ; \quad 0 < f(n) < 1. \qquad (14)$$

The first term on the right hand side of Eq. (14) appears also in renewal files; yet, the term $f(n)$ is unique. $f(n)$ is the probability that accounts for the fact that for moving n anomalous independent particles in the same direction, when these particles indeed try jumping in the same direction (expressed with the term, $< |r| > \sim < |r| >_{free}/n$), the particles in the periphery must move first so that the particles in the middle of the file will have the free space for moving, demanding faster jumping times for those in the periphery. $f(n)$ appears since there is not a typical timescale for a jump in anomalous files, and the particles are independent, and so a particular particle can stand still for a very long time, substantially limiting the options of

progress for the particles around him, during this time. Clearly, $0 < f(n) < 1$, where $f(n) = 1$ for renewal files since the particles jump together, yet also in files of independent particles with $\alpha > 1$, since in such files there is a typical timescale for a jump, considered the time for a synchronized jump. We calculate $f(n)$ from the number of configurations in which the order of the particles' jumping times enables motion; that is, an order where the faster particles are always located towards the periphery. For n particles, there are $n!$ different configurations, where one configuration is the optimal one; so, $\frac{1}{n!} \leq f(n)$. Yet, although not optimal, propagation is also possible in many other configurations; when m is the number of particles that move, then, $f(n) \sim \binom{n}{m}(n-m)!\frac{1}{n!}$, where $\binom{n}{m}(n-m)!$ counts the number of configurations in which those m particles around the tagged one have the optimal jumping order. Now, even when $m \sim n/2$, $f(n) \sim e^{-n/2}$. Using in Eq. (13), $f(n) \sim e^{-n/n_0}$ (n_0 a small number larger than 1), we see,

$$MSD \sim \left(\frac{\alpha}{n_0}\right)^2 ln^2\,(t)\,. \qquad (15)$$

(In Eq. (15), we use, $MSD \sim MAD^2$.) In Fig. 4, we show that results from simulations coincide with Eq. (14), for various values of α. Equation (15) shows that asymptotically the particles are extremely slow in anomalous files of independent particles.

Numerical results of anomalous files of independent particles.- For figuring out even better the effect of this slowness in the scaling of the *MSD* on the level of the file, we perform extensive numerical simulations of anomalous files of independent particles. In the simulations, $N = 501$, and the initial density is a constant with a distance of unity among the point particles. At the edges, reflecting boundaries are positioned at points, ± 253. (We use units without dimensions all

over). Random jumping distances are distributed uniformly in about a unit interval centered on the origin,

$$Jumping\ ditsnace = \sqrt{2Ddt}(2q-1),$$

where q is a random number in the unit interval. The reflection method is used in moving the particles, namely, a jump is made and the particles' order remains.

Trajectories from simulations are shown in Fig. 4. Simulations were performed for ten values of α in the range of anomaly, $0.024 \leq \alpha \leq 0.9$ (in this range, the average of $\psi_\alpha(t)$ is infinite),

$\alpha = 0.024, 0.1, 0.2, 0.3, 0.4, 0.5, 0.6, 0.7, 0.8, 0.9.$

In addition, we performed two control simulations: one for a file of independent particles with $\alpha = 3.37$ [that has a finite average for $\psi_\alpha(t)$] and one for normal dynamics.

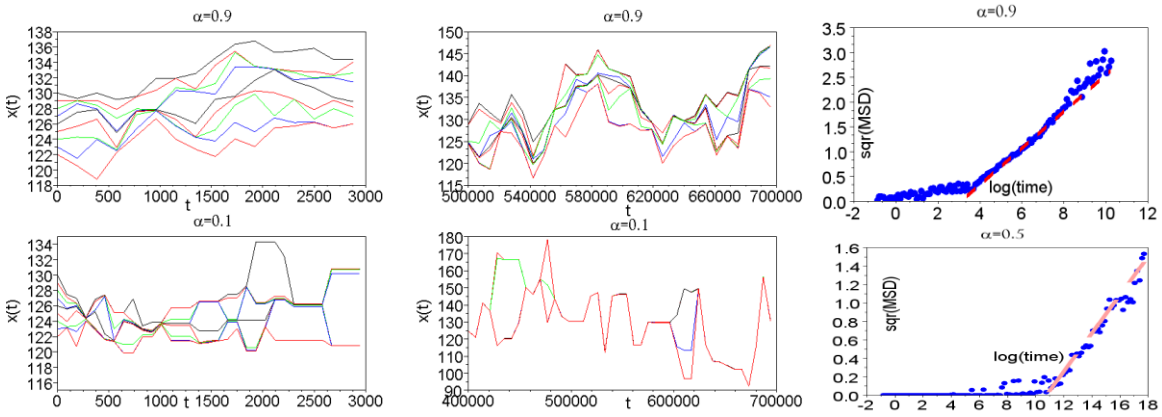

Fig 4 Nine trajectories from anomalous file of independent particles plotted as a function of the cycle index, t; note that the actual time obeys the formula: $t \approx \mathrm{t}^{1/\alpha}$. Particles are initially positioned at the integers, here shown particles located initially in the range, 122-130. In the simulations, $N = 501$, $\Delta = 1$ (the initial distance among particles), $D = 1$ (the diffusion coefficient of the particles), $dt = 0.13$, and the jumping distance obeys, $\sqrt{2Ddt}(2q-1)$, where q is a random number uniform in the unit interval. (Here, we use units without dimensions.) The upper panels show trajectories for $\alpha = 9/10$ and the lower panels for $\alpha = 5/10$. Left panels show high resolution trajectories at the initial stage of the process. Right panels show trajectories at low resolution at the last third of the simulation (we plot the trajectory every seven thousand cycles). Trajectories in a cluster look in this plot as one trajectory. Clearly, trajectories attract each other stronger at small values of α. This is evident at short times and at large times. We also show the *MSD* for two values of α with fitting functions taken from Eq. (15).

Trajectories obtained from simulations are shown in Fig. 4 as a function of the number of the cycles t, where a cycle contains N attempts of jumping. The trajectories exhibit the phenomenon of clustering: namely, particles attract each other and then move pretty much together. It is also evident that the value of α and the number of cycles determine the degree of clustering in the system. We note that the results presented here are independent of the value for N and are qualitative identical for files with finite size particles (see the next paragraph, dealing with additional numerical results).

Characterizing the formation of the clusters, Fig. 5A shows $p_n(\mathrm{t},\alpha)$: the percentage of particles in a cluster at t for a particular α; namely, the number of particles in clusters above the total number of particles. Here, when adjacent particles are at a distance not larger than 0.1, they are considered clustered. The curves height depends on α, yet when normalizing $p_n(\mathrm{t},\alpha)$ with $\xi(\alpha)$ $[\equiv p_n(\mathrm{t}\to\infty,\alpha)]$, the curves pretty much coincide with each other (Fig. 5B). In action, $\xi(\alpha)$ is the average of the last 10% of the trajectory. $\xi(\alpha)$ is shown in Fig. 5C with the optimal (4-parameter) fitting function, $\tilde{\xi}(\alpha)=0.98\left(1-\left(\frac{\alpha}{0.99}\right)^{3.09}\right)^{0.537}-0.028$. This fitting function is of the form of,

$$\tilde{\xi}(\alpha)\approx\sqrt{1-\alpha^3}. \qquad (16)$$

When $\alpha\to 0$, almost all particles are in clusters. The fluctuations in $\xi(\alpha)$ are about 5% for $\alpha=0.9$, and are about 0.5% for $\alpha=0.024$ (with about a linear interpolation with α). The fluctuations in $\xi(\alpha)$ represent the motion of particles among clusters. Namely, for a small value of α at steady state, the particles in a cluster move together, where at larger values of α, about 5 percents of the particles diffuse among clusters. Since clustering occurs only for anomalous α, $\tilde{\xi}(\alpha)$ describes the criticality of a phase transition. Indeed, $\tilde{\xi}(\alpha)$ has a typical form for a scaling

function in critical phenomena [3.7] (see the next paragraph for further discussion about this point)

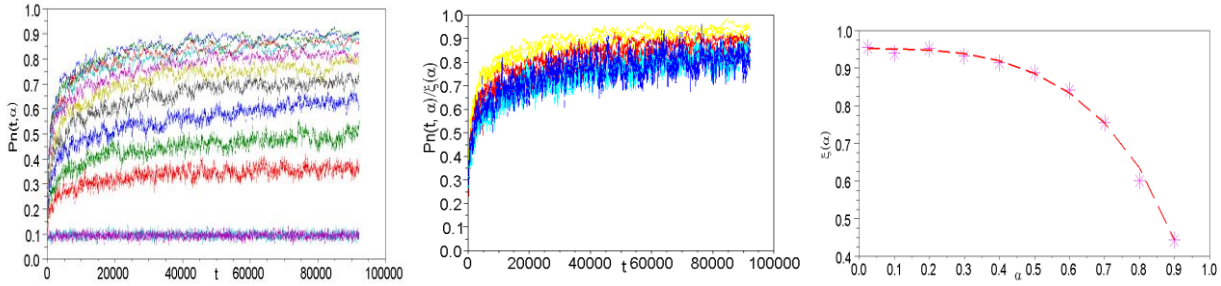

Fig 5 $p_n(\mathrm{t},\alpha)$, its normalized form and $\xi(\alpha)$. (**A**) $p_n(\mathrm{t},\alpha)$ as a function of the event index t, for 10 values of anomalous α, $\alpha = 0.9, 0.8, 0.7, 0.6, 0.5, 0.4, 0.3, 0.2, 0.1, 0.024$, for the third (from the bottom) and on curves respectively, and the control curves: an anomalous file with $\alpha = 3.37$ and a normal dynamics file (these curves are most lower ones and pretty much coincide with each other). The clustering phenomenon is unique for anomalous files of independent particles, representing a phase-transition depending on α. (**B**) Normalizing $p_n(\mathrm{t},\alpha)$ with its asymptotic value $\xi(\alpha)$, all curves follow pretty much the same route. (**C**) $\xi(\alpha)$ is shown on the right with its fitting curve, $\tilde{\xi}(\alpha)$. As α goes to zero, about 97% of the particles are in clusters.

Complementary information about the clustering is obtained from two additional functions: $p_c(\mathrm{t},\alpha)$ and $S_c(\mathrm{t},\alpha)$. Figure 6A presents $p_c(\mathrm{t},\alpha)$: the percentage of clusters at t for a particular α, measured in terms of the number of particles. For relatively large values of α, the number of clusters is also large, yet, the clusters are smaller in size. The fluctuations in the number of clusters is also larger when α is larger. This is in accordance with the behavior of $p_n(\mathrm{t},\alpha)$. Panel 6B shows $\pi(\alpha)$ $[\equiv p_c(\mathrm{t}\to\infty,\alpha)]$ versus α for all anomalous values of α. The optimal fitting function has the form, $\tilde{\pi}(\alpha) = 0.78\left(1+\left(\frac{\alpha}{1.19}\right)^{2.49}\right)^{0.42} - 0.75$. $\tilde{\pi}(\alpha)$ follows closely a function of the form,

$$\tilde{\pi}(\alpha) \approx 0.6\left(\sqrt{1.7+\alpha^3}-1.25\right). \quad (17)$$

$\tilde{\xi}(\alpha)$ and $\tilde{\pi}(\alpha)$ have complementary physical interpretation, seen in their scaling laws following (about), $\sqrt{1 \pm \alpha^3}$. $\tilde{\xi}(\alpha)$ quantifies particles in clusters, where the same number of particles can exist for a small or a large number of clusters. $\tilde{\pi}(\alpha)$ simply counts clusters, and can have the same value when these are either small clusters or large clusters. Importantly, when clustering occurs, we see a small number of large clusters as α becomes smaller, where in a system without clustering, we may see about 10% of small clusters.

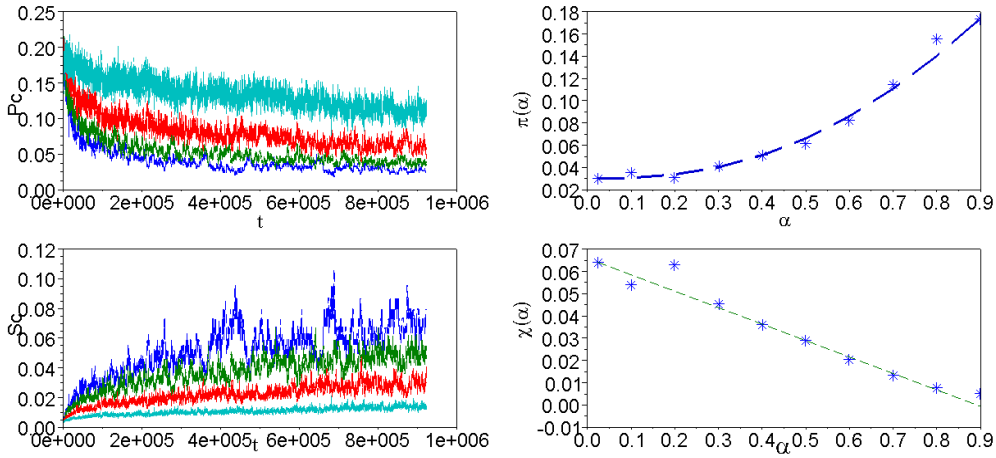

Fig 6 $p_c(\mathrm{t},\alpha)$, $\pi(\alpha)$, and $S_c(\mathrm{t},\alpha)$ and, $\chi(\alpha)$. (**A**) $p_c(\mathrm{t},\alpha)$ as a function of the event index t, for 4 values of anomalous α, $\alpha = 0.7, 0.5, 0.3, 0.024$, counting from the top curve. The percentage of clusters is smaller when α is small, since the clusters are larger at small α. (**B**) $\pi(\alpha)$, the steady state value for the number of clusters in percentages is shown with its fitting curve, $\tilde{\pi}(\alpha)$. As $\alpha \to 0$, the percentage of clusters is 3%. (**C**) $S_c(\mathrm{t},\alpha)$ as a function of the event index t, for the 4 values of anomalous α in (**A**), counting from the lower curve. The average size of a cluster is large when α is large. Here, the average cluster can contain, momentarily, about 10% of the particles. (**D**) $\chi(\alpha)$, the steady state value for the average size of a cluster (in percentage) with its simple fitting curve, $\tilde{\chi}(\alpha)$. As $\alpha \to 0$, the average cluster's size is 33.

Figure 6C presents the average size of a cluster, $S_c(\mathrm{t},\alpha)$ [$\equiv p_n(\mathrm{t},\alpha)/p_c(\mathrm{t},\alpha)$]. Here, fluctuations are larger when α is small. Panel 6D shows $\chi(\alpha)$, the asymptotic value of the a cluster's size, $\chi(\alpha) = S_c(\mathrm{t}\to\infty,\alpha)$, with its simple fitting function,

$$\tilde{\chi}(\alpha) = (33 - 37\alpha)/N. \qquad (18)$$

Interestingly, the average size of a cluster is limited with about 33 particles when $\alpha \to 0$, where clustering disappears when $\alpha \to 1$, further quantifying the phase transition.

Additional Numerical Results: a large file and a file with finite size particles.- In this part, we show results for a file with several thousand particles and for a file with finite size particles. The behavior of these files coincide with the behavior of the file reported in the previous part; namely, clustering is indeed a stable phenomenon in anomalous files of independent particles and holds in small and large files and in files of point particles and of finite size particles.

Files with finite size particles.- Firstly, we present results in an anomalous file of independent particles of finite size. In the simulations, each particle is of a size of 0.01. (We use quantities without dimension all over.) Initially, N particles are located in a symmetric way around the origin at a distance of 1.11 from each other, where $N = 2M + 1$ and here $M = 237$. Each actual jump obeys, $\sqrt{2Ddt}(2q-1)$, where $D = 1$, $dt = 0.13$, and q is a random number taken from the unit interval. After each jump the particles are ordered, and are moved such that they are not overlapping. When adjacent particles are at a distance not larger than 0.1329, they are considered clustered.

We report on results for $p_n(\mathrm{t},\alpha)$ and $\xi(\alpha)$, $p_c(\mathrm{t},\alpha)$ and $\pi(\alpha)$ and $S_c(\mathrm{t},\alpha)$ and $\chi(\alpha)$. We recall:

- $p_n(\mathrm{t},\alpha)$: the number of particles in clusters over the total number of particles as a function of t and α.

- $\xi(\alpha) \equiv p_n(\mathrm{t} \to \infty, \alpha)$, calculated as the average of the last 10% of the trajectory
- $p_c(\mathrm{t}, \alpha)$: the number of clusters over the total number of particles as a function of t and α
- $\pi(\alpha) \equiv p_c(\mathrm{t} \to \infty, \alpha)$, calculated as the average of the last 10% of the trajectory
- $S_c(\mathrm{t}, \alpha)$: the average number of particles in a cluster as a function of t and α
- $\chi(\alpha) \equiv S_c(\mathrm{t} \to \infty, \alpha)$, calculated as the average of the last 10% of the trajectory

We note that the results reported here were tested with several types of algorithms for simulating finite size particles. It is important using a continuous coordinate and a continuous-motion-technique (jumps are made and then the particles are ordered and moved such that they are not overlapping). Nevertheless, this is the most physical way of simulating finite size particles in a file, since particles in nature move in a continuous way, and when they bump each other they can exchange momentum for an incremental distance (in a medium of a finite temperature).

Figure 7 shows $p_n(\mathrm{t}, \alpha)$ (left panel) as a function of t for several values of α,

$\alpha = 0.024, 0.1, 0.3, 0.5, 0.7, 0.9, 3.37,$

and its steady function $\xi(\alpha)$ as a function of α (right panel). The forms of these quantities coincide with the forms of the corresponding quantities in files of point particles. In particular, the fitting function for $\xi(\alpha)$, $\tilde{\xi}(\alpha)$, follows the form,

$$\tilde{\xi}(\alpha) = 0.8492\left(1 - \left(\frac{\alpha}{0.99}\right)^{3.09}\right)^{0.537} - 0.028. \qquad (19)$$

This is a particular case of the general formula used also for point particles,

$$\tilde{\xi}(\alpha) = c_1\left(1 - \left(\frac{\alpha}{c_2}\right)^{\mu_{\tilde{\xi}}}\right)^{\nu_{\tilde{\xi}}} - c_3. \qquad (20)$$

Excluding the first parameter c_1, that here equals, $c_1 = 0.8492$ and equals, $c_1 = 0.98$, for point-like particles, $\tilde{\xi}(\alpha)$ is identical in both cases.

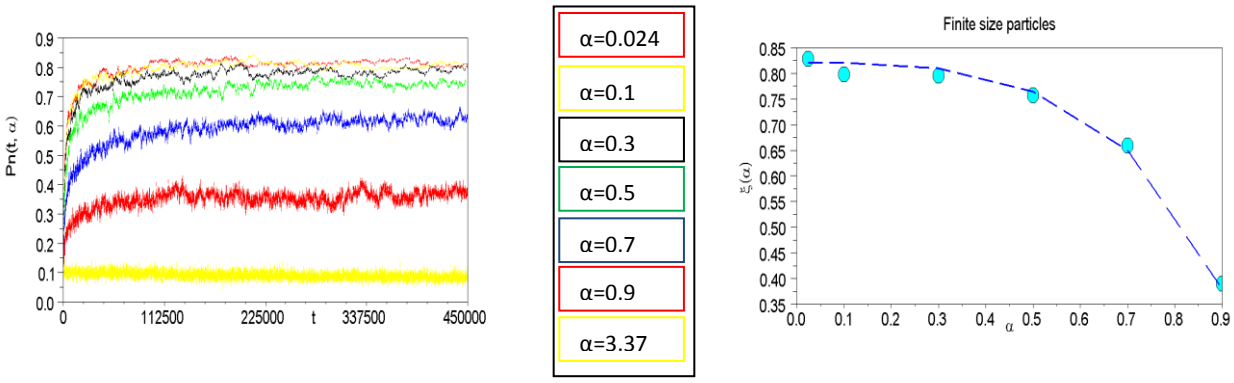

Fig 7 $p_n(\mathrm{t},\alpha)$ (left panel) as a function of the cycle index t for 7 values of α (specified in the middle panel) and its steady state function $\xi(\alpha)$ (right panel) from trajectories of files of anomalous, independent, particles of finite size. In the simulations, $N = 501$, the size per particle is 0.01, $\Delta = 1.11$ (the initial distance among particles), $D = 1$ (the diffusion coefficient of the particles), $dt = 0.13$, and the jumping distance obeys, $\sqrt{2Ddt}(2q-1)$, where q is a random number uniform in the unit interval. (Here, we use unite without dimensions.) Reflecting boundaries are positioned at a distance of 27 integers relative to the initial position of the particles at the edges, in the direction that extends the interval. When adjacent particles are at a distance not larger than 0.1329, they are considered clustered. $p_n(\mathrm{t},\alpha)$ and $\xi(\alpha)$ have the same form seen in the case of point particles, yet here, $\xi(\alpha \to 0)$ has a smaller value of about 5 percent relative to a file of point particles.

Now, figure 8 shows the behavior of $p_c(\mathrm{t},\alpha)$ and $\pi(\alpha)$, and $S_c(\mathrm{t},\alpha)$ and $\chi(\alpha)$ for finite size particles. The fitting function for a file of $\pi(\alpha)$, $\tilde{\pi}(\alpha)$, follows the form,

$$\tilde{\pi}(\alpha) = 0.82\left(1+\left(\frac{\alpha}{1.19}\right)^{2.49}\right)^{0.29} - 0.75. \qquad (21)$$

Again, this fitting function $\tilde{\pi}(\alpha)$ obeys the exact same general form as in a file of point-like particles,

$$\tilde{\pi}(\alpha) = p_1\left(1+\left(\frac{\alpha}{p_2}\right)^{\mu_{\tilde{\pi}}}\right)^{\nu_{\tilde{\pi}}} - p_3. \qquad (22)$$

Here the difference is in p_1 ($p_1 = 0.82$ here and $p_1 = 0.78$ in a file of point-like particles) and in $\nu_{\tilde{\pi}}$ ($\nu_{\tilde{\pi}} = 0.29$ here and $\nu_{\tilde{\pi}} = 0.42$ in point-like particles). The fitting function for the average number particles in a cluster $\chi(\alpha)$, $\tilde{\chi}(\alpha)$, obeys,

$$\tilde{\chi}(\alpha) = (12.29 - 11\alpha)/N. \quad (23)$$

Again, this is the a particular case of the general form,

$$\tilde{\chi}(\alpha) = (\tilde{\chi}_0 - x\alpha)/N, \quad (24)$$

found also for point particles. Both parameters of the linear function $\tilde{\chi}(\alpha)$ are three times smaller here compared with the case of point particles; mathematically, this is a direct consequence of the difference in the parameters of $\tilde{\pi}(\alpha)$ among the files: since the number of clusters is larger here (2.9 times larger), yet the total number of particles in clusters is about equal, the average number of particles in a cluster is smaller (about one third).

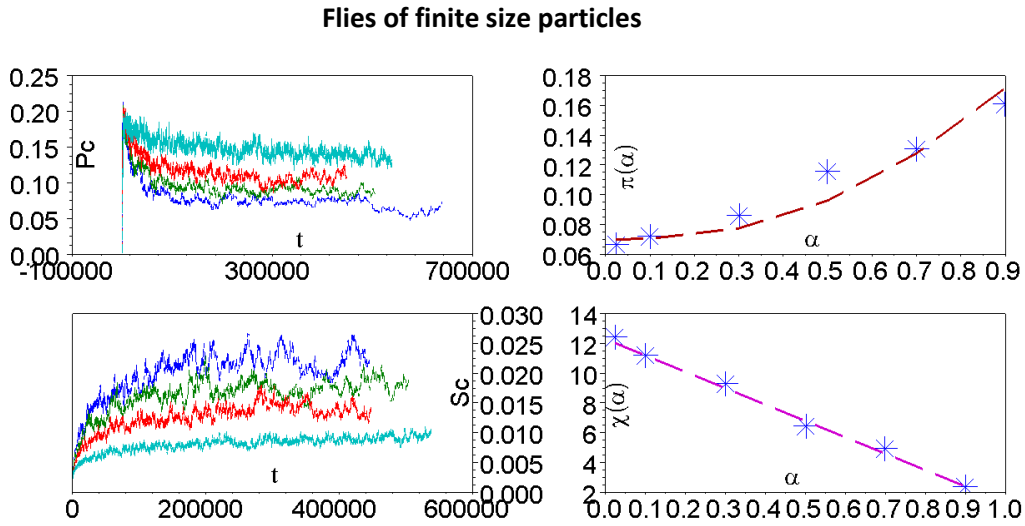

Fig 8 *Finite size particles.-* $p_c(\mathrm{t},\alpha)$ (upper left panel) as a function of the cycle index t for several values of α ($\alpha = 0.024, 0.3, 0.5, 0.7$ from the lower curve) and its steady state function $\pi(\alpha)$ (upper right panel), $S_c(\mathrm{t},\alpha)$ (lower left panel, where here, curves with smaller values of α are on top) and its steady state function, $\chi(\alpha)$. $\pi(\alpha \to 0)$ is about three times larger in finite size particle file, and $\chi(\alpha)$ is three times smaller.

A larger file.- Here, we examine the behavior of a file with several thousand particles. Initially, N particles are located in a symmetric way around the origin at a distance of 1 from each other, where $N = 2M + 1$ and here $M = 1137$ (this file is about five times larger than the files

presented in the previous paragraphs). The fastest particle attempts a jump, and the random times are adjusted. Each actual jump obeys, $\sqrt{2Ddt}(2q-1)$, where $D=1$, $dt=0.13$, and q is a random number taken from the unit interval. After each jump the particles are ordered. Reflecting boundaries were placed at a distance of unity from the particles at the edges in the direction that extends the interval. When adjacent particles are at a distance not larger than 0.1, they are considered clustered. Results were collected for the following values of α,

$$\alpha = 0.1, 0.3, 0.5, 0.7, 0.9, 3.37. \quad (25)$$

The results are reported in Fig. 9 showing $\xi(\alpha)$, $\pi(\alpha)$, and $\chi(\alpha)$, and their fitting functions.

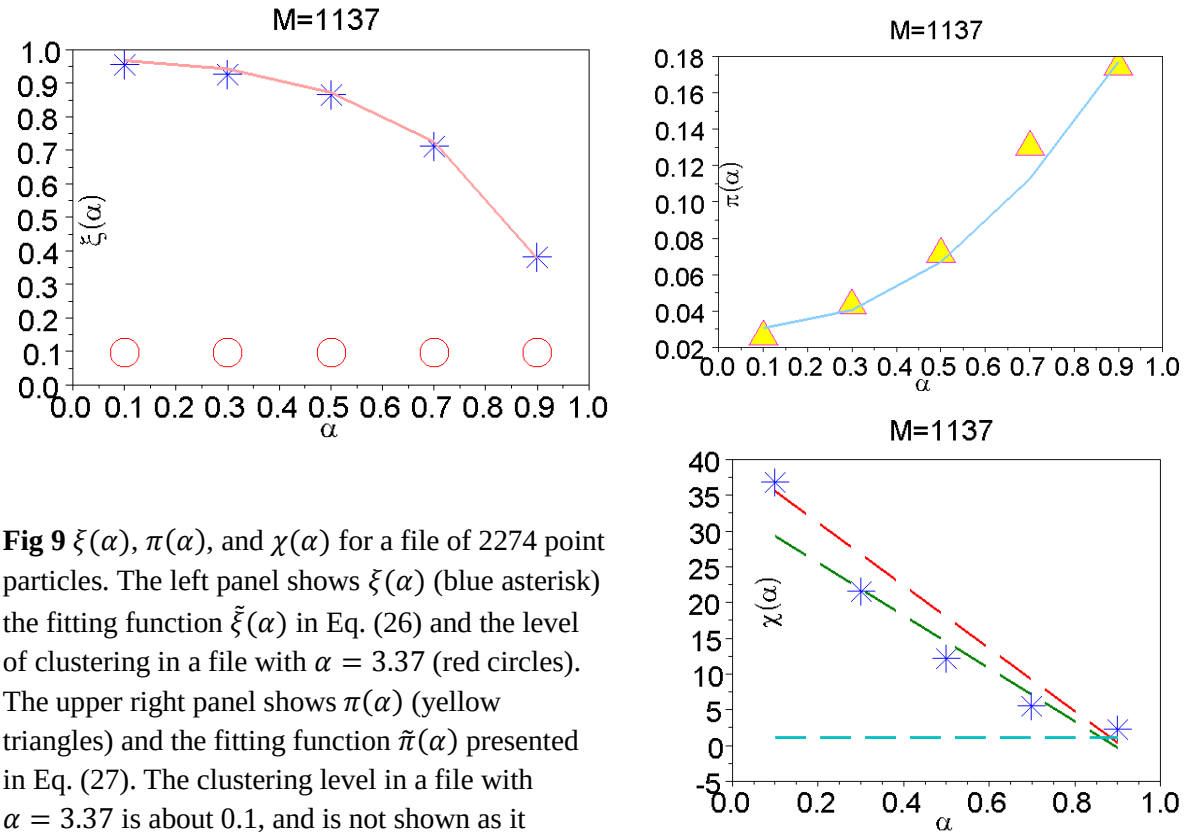

Fig 9 $\xi(\alpha)$, $\pi(\alpha)$, and $\chi(\alpha)$ for a file of 2274 point particles. The left panel shows $\xi(\alpha)$ (blue asterisk) the fitting function $\tilde{\xi}(\alpha)$ in Eq. (26) and the level of clustering in a file with $\alpha = 3.37$ (red circles). The upper right panel shows $\pi(\alpha)$ (yellow triangles) and the fitting function $\tilde{\pi}(\alpha)$ presented in Eq. (27). The clustering level in a file with $\alpha = 3.37$ is about 0.1, and is not shown as it represents only very small clusters, and doesn't reflect the clustering phenomenon that the function $\pi(\alpha)$ represents (small values in $\pi(\alpha)$ stands for very large clusters). The lower right panel shows $\chi(\alpha)$ (blue asterisks) the fitting function in Eq. (28), red dashed curve, the fitting function $\tilde{\chi}(\alpha)$ of the smaller file (green dashed curve), and the average size of a cluster in a file with $\alpha = 3.37$ (the light blue horizontal dashed line).

The fitting functions of $\xi(\alpha)$, $\pi(\alpha)$, and $\chi(\alpha)$, obey the same general formula introduced in Eqs. (20), (22), (24), respectively. In particular, we find the following fitting functions:

- $\tilde{\xi}(\alpha) = 1.1\left(1 - \left(\frac{\alpha}{0.96}\right)^{2.416}\right)^{0.4} - 0.13.$ (26)
- $\tilde{\pi}(\alpha) = 0.98\left(1 + \left(\frac{\alpha}{1.15}\right)^{2.2}\right)^{0.3} - 0.95.$ (27)
- $\tilde{\chi}(\alpha) = 39.99 - 43.99\alpha.$ (28)

These results are in accordance with the results of the smaller file. Namely, the clustering is independent of the number of walkers in the file, and thus it is a general phenomenon.

III.b.3. Discussion on anomalous files of independent particles

Characterizations of the clustering.- Firstly, we recall that slowness is expected in files of anomalous independent particles since the order of the jumps that enables motion is exponentially small (with the number of particles that are suppose moving) and the dynamics are without a typical timescale. For further explaining the clustering, we look on the actual values of the jumping times of the particles after a while that the process has been going on; see Fig.10. (These are the quantities discussed in the derivation of the *MSD*, around Eq. (15).) It is clear from Fig. 10 that when α decreases the typical value for a jumping time increases (here, the typical time is the jumping time of most of the particles). The interesting issue here is that when α decreases there is a phenomenon that only a few particles are significantly faster relative to all the others. This tells the story of the clustering and the phase transition: when one particle jumps over and over and over again, it clusters the particles around him, since when only a particular particle moves repeatedly several times, it closes the gap among the particles around him among themselves, such that they are and eventually clustered.

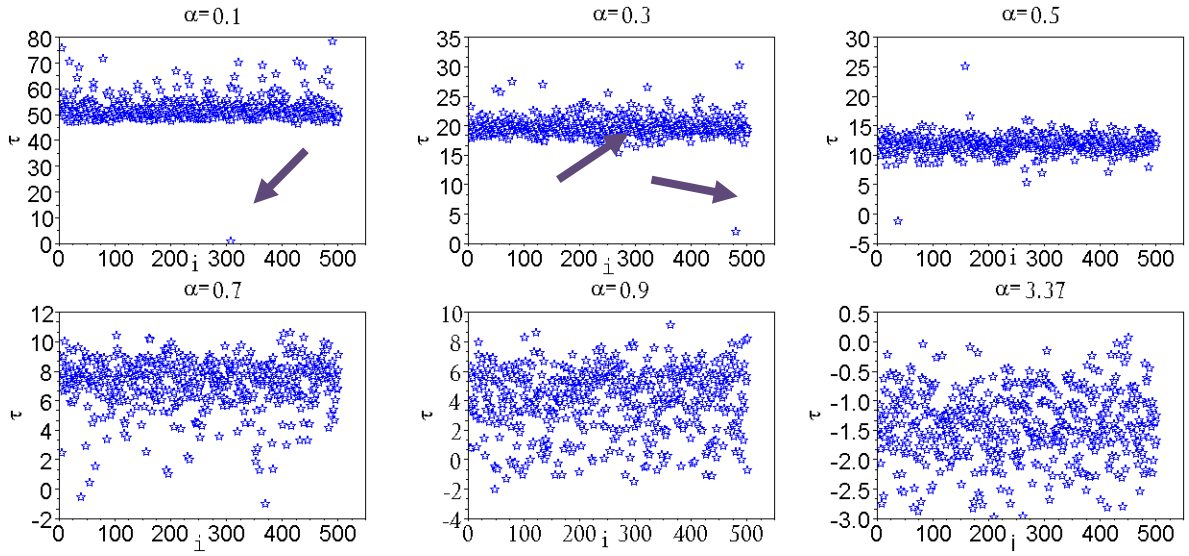

Fig 10 The logarithm of the band of jumping times after about 7 hundred thousand cycles for a system of about 500 point particles for several values of α. The arrows indicate on the fast jumping times in the range considered small α values ($\alpha < 0.5$).

How can we explain the form of the fitting functions? Firstly, we note that the fitting function of $\xi(\alpha)$ has a standard form for a scaling function at criticality of a phase transition [3.7]: $f(\alpha)\sim(1-\alpha)^{\mu}$ (where a function in α can replace α in generalizations). $\chi(\alpha)$ and $\pi(\alpha)$ pretty much follow from $\xi(\alpha)$. $\pi(\alpha)$ is complementary to $\xi(\alpha)$, since it has such a physical interpretation, and $\chi(\alpha)$ is the ratio of the previous ones.

Now, for further supporting the form of the fitting function of $\xi(\alpha)$, we calculate the PDF of slowest jumping time when there are $n+1$ jumping times in the band:

$$f_{s.t.}(t;n+1)=\psi(t)\left(\int_0^t\psi(s)ds\right)^n\sim t^{-1-\alpha}e^{-nt^{-\alpha}}. \qquad (29)$$

We emphasize the following three points:

(1) $f_{s.t.}(t;n+1)$ is very small for times smaller than, $t^* \equiv n^{1/\alpha}$, that is the time when the argument of the exponent $e^{-nt^{-\alpha}}$ is unity.

(2) t^* is the typical timescale for most of the particles in the file, in the limit of many cycles. This is indeed seen in Fig. 10. The reason is very simple: after many cycles, most of the particles are extremely slow, since only the fast ones move and after several jumps the anomalous properties of $f_{s.t.}(t;n+1)$ 'assign' the particle a very slow jumping time.

(3) When calculating the first and the second moments of $f_{s.t.}(t;n+1)$ in the range $t \leq t^*$, we find, $< t > \sim n^{1/\alpha-1}$ and $< t^2 > \sim n^{1/\alpha-2}$. This should reflect the properties of the fast particles until the time t^*. It is evident that a transition occurs in the second moment when $\alpha > 1/2$: $< t^2 >$ vanishes when $\alpha > 1/2$, yet scales with n when $\alpha < 1/2$. Namely, for $\alpha < 1/2$ many of the (relative) fast particles are slower than t^*, yet when $\alpha > 1/2$, most of the (relative) fast particles are indeed faster than t^*. This behavior is indeed seen in Fig. 10: when $\alpha < 1/2$ fewer and fewer particles are seen in the range $t \leq t^*$, yet when $\alpha > 1/2$ we see many particles in this range. This is reflected in the behavior of the file: the file contains many small clusters when $\alpha > 1/2$, yet only a few clusters, nevertheless larger, when $\alpha \leq 1/2$. $\tilde{\xi}(\alpha)$ and $\tilde{\pi}(\alpha)$ capture this property.

Anomalous files in two dimensions.- Now, we also find that clustering is seen in anomalous files embedded in two-dimensions, creating a network of isotropic files, like streets and junctions in a city (see Fig. 11). Indeed, this system is a generalization of a one-dimensional file studied throughout this chapter, and it is defined with two free parameters: the percentage of intersections (without directional preference in intersections) and the length of the interval until an intersection occurs. We study files that intersect each other for 1% every interval of 10 (see

the comprehensive analysis in the next paragraph). Among other results, we find that in such a system 50% of the particles are in clusters when $\alpha \to 0$. Indeed, the results are sensitive to the branching parameters: when branching occurs in smaller intervals, clustering decreases, and we can speculate that when diffusion happens in two dimensions (not in a network of one-dimensional files), the clustering phenomenon is not observed when the density is reasonable (not too high). This is in accordance with known results showing that the slower diffusion so typical for a particle in a file in one-dimension does not hold for diffusion of hard particles in two-dimensions, where in such a system a standard diffusion is seen (when the density is not too high). Still, we have chosen here reasonable parameters for the branching: the average size of a jump is 0.25, and the branching occurs every interval of 10; this is not too small interval so branching indeed has a role (seen also in the results), still the branching happens after frequent enough jumps and the clustering is indeed seen.

Analysis of anomalous files embedded in two dimensions.- Here, we test the occurrence of the clustering phenomenon in an ordered network of files embedded in two dimensions forming an isotropic network of files and junctions. This system can mimic diffusion in a membrane that has many obstacles for the diffusing objects, forming streets and junctions. We show that clustering occurs also in this system. Indeed, further study of the dynamics of independent anomalous particles in files embedded in two-dimensions and even in three-dimensions is needed; still, from the results reported here we can related the critical phenomenon of clustering with rafts in membranes. This is discussed in the next title, where here we present the results from the simulations.

In files embedded in two dimensions, we have two free parameters defining the system: the percentage of intersections and the length of the interval until an intersection occurs. In the current system, files intersect each other only 1% of the time, every interval of 10 (see figure 11 for an illustration).

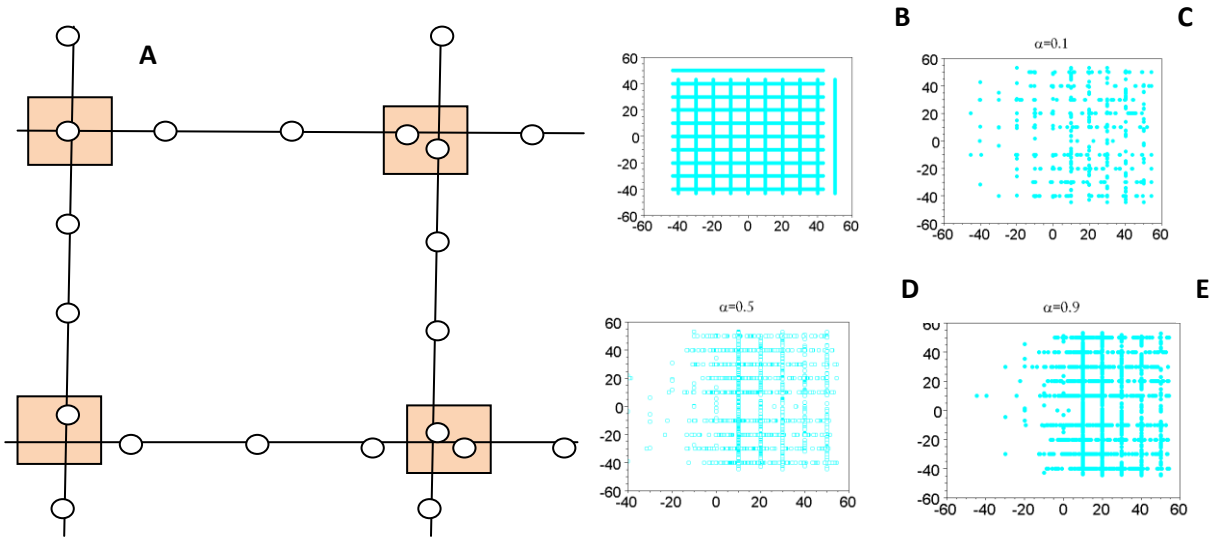

Fig 11 (**A**) An illustration of files embedded in two dimensions, with 1% branching every interval of 10. At the end of every interval of length 10 in a given direction there is a possibility for branching for a length of 0.1 (the colored squares). Here, particles are marked with circles. (**B-E**) Here, we present the particles at the initial stage of the process (**B**) and at the end of process (after about 733 thousands cycles), for $\alpha = 0.1$ (**C**) $\alpha = 0.5$ (**D**), and $\alpha = 0.9$ (**E**). In these plots, a cluster is seen as a dense area of particles with areas free of particles around it.

Mathematically, we define files in two dimensions in an area $A(x, y)$: in x-files, x is a continuous coordinate, and y is an integer, $y = 0, \pm 4, \pm 8, \pm 12, \ldots$ In y-files, set $x \leftrightarrow y$. In the simulations, 1980 particles were located in 20 one-dimensional files: 10 x-files (constant y) and 10 y-files (constant x). In each file there are 99 particles; the particles are located around the origin, in a symmetric way, a particle every 0.88. At about, $x, y = \pm 52$, we put reflecting

boundaries. See Fig. 11 for an illustration of the system, the initial configuration and the final configuration for various values of α in the area $A(x,y)$ after several thousand cycles.

The quantities $p_n(\mathrm{t},\alpha)$ and $\xi(\alpha)$ and $p_c(\mathrm{t},\alpha)$ and $\pi(\alpha)$ and $S_c(\mathrm{t},\alpha)$ and $\chi(\alpha)$ are calculated for this system, and are presented in Fig. 12. Results are calculated for,

$$\alpha = \ 0.1, 0.3, 0.5, 0.7, 0.9, 3.37. \qquad (30)$$

Figure 12 shows the quantities $p_n(\mathrm{t},\alpha)$, $p_c(\mathrm{t},\alpha)$ and $S_c(\mathrm{t},\alpha)$ calculated in a similar way for files embedded in one dimension: each one dimensional file (with a constant x or a constant y) is calculated as an independent file, clustering is when particles are at a distance of 0.11 or smaller, and then an average is applied. The familiar forms of these quantities seen in files embedded in one dimension are observed also in files embedded in two-dimensions with 1% branching every interval of 10. Namely, clustering occurs even when the files are embedded in two dimensions.

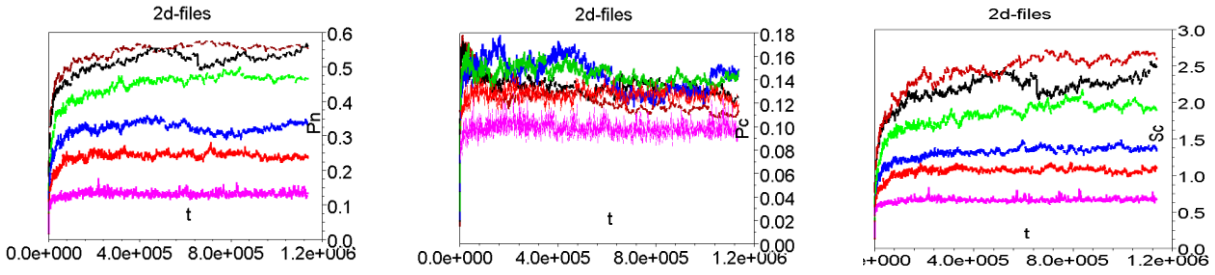

Fig 12 $p_n(\mathrm{t},\alpha)$, $p_c(\mathrm{t},\alpha)$ and $S_c(\mathrm{t},\alpha)$ for anomalous files of independent particles embedded in two dimensions with 1% branching every interval of length 10. In the left panel, shown is $p_n(\mathrm{t},\alpha)$ for α values presented in Eq. (30) (curves with larger values of α are of smaller height). The middle panel shows $p_c(\mathrm{t},\alpha)$; each curve with a particular α has the same color used its counterpart $p_n(\mathrm{t},\alpha)$ shown in the left panel. Here, the number of clusters is about the same for all values α, and this means that the clustering is a bit weaker here relative with the clustering of a file embedded in one dimension. There are a lot of free particles and a lot of small clusters. This is seen explicitly in the right panel when plotting the number of particles in a cluster versus t for the various values of α. Clusters are indeed smaller relative with files embedded in one dimension, still there is a prominent effect of an increase in the average number of particles in a cluster when α decreases.

Figure 13 quantifies further the clustering in files in two dimensions when showing the quantities $\xi(\alpha)$, $\pi(\alpha)$ and $\chi(\alpha)$. The fitting functions show that the branching affects the degree of clustering: here, 55% of the particles (relative to a file in one dimension) are in clusters. Still, when comparing the results in the two dimensional system for the various values of α, we see that when $\alpha \to 0$, the percent of clustering is five times larger compared with $\alpha = 3.37$. This indicates on a prominent clustering in anomalous files of independent particles in two dimensions relative with other files' types in two dimensions.

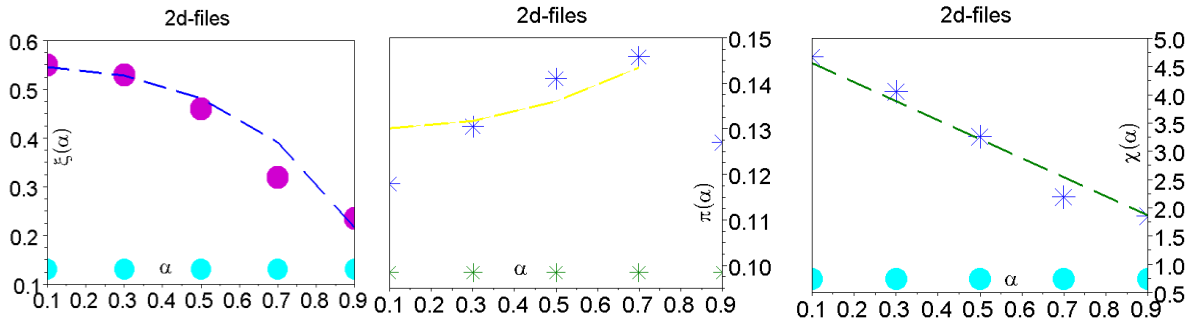

Fig 13 $\xi(\alpha)$, $\pi(\alpha)$, and $\chi(\alpha)$ for files embedded in two dimensions with 1% branching every interval of 10. In every figure the horizontal curve stands for the result for $\alpha = 3.37$. The fitting curves for $\pi(\alpha)$ is obtained for the first 4 points excluding the fifth. For the specific forms of the fitting functions, see Eqs. (31)-(33). These plots show that clustering is indeed seen in 2d-files with 1% branching every interval of 10.

The fitting functions shown in Fig. 13 obey the formulae in Eqs. (20), (22), (24), of the file embedded in one dimension:

$$\tilde{\xi}(\alpha) = 0.55\left(1 - \left(\frac{\alpha}{0.99}\right)^{2.374}\right)^{0.577} - 0.0028. \qquad (31)$$

$\tilde{\pi}(\alpha)$ follows:

$$\tilde{\pi}(\alpha) = 0.13\left(1 + \left(\frac{\alpha}{1.19}\right)^{2.505}\right)^{0.42}. \qquad (32)$$

$\tilde{\chi}(\alpha)$ follows:

$$\tilde{\chi}(\alpha) = 4.9 - 3.37\alpha. \quad (33)$$

The fact that the fitting functions obey the same general formula seen in the one dimensional files further support the occurrence of the clustering in an isotropic network of files embedded in two-dimensions.

Anomalous files, rafts and channels.- An isotropic network of files embedded in two-dimensions enables relating the clustering with rafts: a raft in a (two-dimensional) membrane is a dense patch of specific lipo-molecules [3.5]. The mechanism of the formation of these patches is still not clear, yet it is known that rafts do not largely occur due to an electrostatic attraction. We think that the phenomenon of clustering in anomalous files of independent particles can explain rafts in membranes: given that the lipo-molecules diffusion is anomalous (anomalous diffusion is common in membranes), they will form rafts, since diffusion in biological membranes is describable with the model of an isotropic network of files in two dimensions. This statement is based on the known fact that the membrane is composed from a mosaic of areas of different compositions, where these have different viscosities; this may indeed cause the diffusing objects see the diffusion like diffusion in tunnels with junctions (embedded in two dimensions).

Finally, we expect that the clustering phenomenon is universal and holds in a wide range of external conditions, since the diffusion coefficient of the particles does not affect this phenomenon, yet α, the only other external parameter here, is the control parameter. Since clustering is expected universal, it may be used in regulating biological channels, an important

topic in biophysics, e.g. [3.6]; this is achieved when controlling the phase of the anomalous particles in the channel, clustered or diffusing, using one of two possibilities:

- When changing α such that it is either smaller than 1 or larger than 1, we can cause the system having either an infinite typical timescale or a finite typical timescale. For a finite timescale, diffusing is seen, where for an infinite timescale clustering is expected.
- When controlling the synchronization of the particles, either having a file made of synchronized anomalous particles or having a file made of independent anomalous particles, we nicely have the possibility of seeing either a diffusing phase (for synchronized) or a clustered phase (for independent particles).

References

Chapter 1

[1.1] A. Einstein, Annalen der Physik 17 (1905) 549.

[1.2] N. G. van Kampen, *Stochastic Processes in Physics and Chemistry* (revised and enlarged edition, North-Holland, Amsterdam, 1992).

[1.3] R. Zwanzig, *Nonequilibrium Statistical Mechanics*, Oxford University Press, NY, 2001.

[1.4] N. W. Goel and N. Richter-Dyn, *Stochastic Models in Biology*, Academic Press, NY, 1974.

[1.5] S. Redner, *A Guide to First-Passage Process*, Cambridge University, 2001.

[1.6] H. Risken, *The Fokker-Planck Equation*, Springer, Berlin, 1984.

[1.7] G. H. Weiss, *Aspects and Applications of the Random Walk*, North-Holland, Amsterdam, 1994.

[1.8] D. R. Cox, *Renewal Theory*, Methuen, London, 1962.

[1.9] B. D. Hughes, *Random walks and random environments*, Clarendon Press, Oxford, New York, 1995.

[1.10] S. Alexander and R. Orbach, J. Phys. (Paris) Lett. 43 (1982) L625.

[1.11] T. M. Liggett, *Interacting Particle Systems*, New York: Springer, 1985.

[1.12] O. Flomenbom and A Taloni, Europhys. Lett. 83 (2008) 20004-p1-p6.

[1.13] O. Flomenbom, Phys. Rev. E. 82 (2010) 031126.

[1.14] O. Flomenbom, Phys. Lett. A 374 (2010) 4331.

[1.15] B. Alberts, D. Bray, J. Lewis, M. Raff, K. Roberts, and J. D. Watson, *Molecular Biology of The Cell*, Garland Publishing, Inc, NY & London, 1994.

[1.16] R. N. Mantegna and H. Eugene Stanley, *An Introduction to Econophysics: Correlations and Complexity in Finance*, Cambridge University Press, Cambridge, UK 2000.

[1.17] O. Flomenbom, Phys. Lett. A **374**, 4331 (2010).

Chapter 2

[2.1] T. M. Liggett, *Interacting Particle Systems* (New York: Springer, 1985).

[2.2] T. E. Harris, J. Appl. Probab. **2**, 323 (1965);

[2.3] D.W. Jepsen, J. Math. Phys. (N.Y.) **6**, 405 (1965); J. L. Lebowitz and J. K. Percus, Phys. Rev. **155**, 122 (1967).

[2.4] D. G. Levitt, Phys. Rev. A **8**, 3050 (1973).

[2.5] C. R¨odenbeck, J. K¨arger and K. Hahn, Phys. Rev. E 57, 4382 (1998).

[2.6] H. van Beijeren *et al.*, Phys. Rev. B **28**, 5711 (1983).

[2.7] M. Kollmann, Phys. Rev. Lett. **90**, 180602 (2003).

[2.8] M.D. Jara and C. Landim, Ann. I.H. Poincar´e - PR 42, 567 (2006).

[2.9] P. Kalinay and J. K. Percus, Phys. Rev. E **76**, 041111 (2007).

[2.10] K. Hahn and J. Ka¨rger, J. Phys. A **28**, 3061 (1995).

[2.11] K. Hahn and J. Ka¨rger, J. Chem. Phys. **100**, 316 (1996).

[2.12] A. Taloni and F. Marchesoni, Phys. Rev. Lett. **96**, 020601 (2006).

[2.13] D. S. Sholl and K. A. Fichthorn, Phys. Rev. E **55**, 7753 (1997).

[2.14] F. Marchesoni and A. Taloni, Phys. Rev. Lett. **97,** 106101 (2006).

[2.15] S. Alexander and P. Pincus, Phys. Rev. B **18**, 2011 (1978).

[2.16] R. Kutner, H. Van Beijeren, and K. W. Kehr, Phys. Rev. B **30**, 4382 (1984).

[2.17] K. Hahn and J. Ka¨rger, J. Phys. Chem. B **102**, 5766 (1998);

[2.18] H. L. Tepper, J. P. Hoogenboom, N. F. A. van der Veget and W. J. Briels, J Chem. Phys. **110**, 11511 (1999).

[2.19] K. K. Mon and J. K. Percus, J. Chem. Phys. **117**, 2289 (2002).

[2.20] L. Lizana and T. Ambjörnsson, Phys. Rev. Lett. **100**, 200601 (2008).

[2.21] C. Aslangul, J. Phys. A: Math. Gen. **33**, 851 (2000); Europhys. Lett. **44**, 284 (1998).

[2.22] K. Hahn *et al.*, Phys. Rev. Lett. **76**, 2762 (1996).

[2.23] J. P. de Gennes, J. Chem. Phys. **55**, 572 (1971).

[2.24] J. Ka¨rger and D. M. Ruthven, *Diffusion in Zeolites and Other Microscopic Solids*, Wiley (NY) (1992).

[2.25] G. Coupier, M. Saint Jean, and C. Guthmann, EPL, **77** (2007) 60001

[2.26] P. H. Nelson, S. M. Auerbach, J. Chem. Phys. **110**, 9235 (1999).

[2.27] B. Lin, M. Meron, B. Cui, S. A. Rice, H. Diamant, Phys. Rev. Lett. **94,** 216001 (2005).

[2.28] R. Shusterman, S. Alon, T. Gavrinyov, and O. Krichevsky, Phys. Rev. Lett. **92**, 048303 (2004).

[2.29] P. Demontis *et al.*, J. Chem. Phys. **120**, 9233 (2004); R. L. June *et al.*, J. Chem. Phys. **94**, 8232 (1990); U. Hong *et al.*, Zeolites **11**, 816 (1991).

[2.30] Q. H. Wei *et al.*, Science **287**, 625 (2000); C. Lutz *et al.*, Phys. Rev. Lett. **93**, 026001 (2004).

[2.31] P. M. Richards, Phys. Rev. B 16, 1393 (1977).

[2.32] O. Flomenbom, *Clustering in anomalous files of independent particles*, in press, Europhys. Lett. (2011).

[2.33] D. R. Cox and D. V. Hinkley, *Theoretical Statistics* (Chapman & Hall/CRC, Boca Raton, 1979).

[2.34] H. A. Bethe, Z. Phys. **71**, 205 (1931).

Chapter 3

[3.1] O. Flomenbom, *Clustering in anomalous files of independent particles*, in press, Europhys. Lett (2011).

[3.2] Bandyopadhyay T., Europhys. Lett., **81** (2008) 16003.

[3.3] M. Granda Valdés, A.I. Pérez-Cordoves and M.E. Díaz-García, Tr. Anal. Chem. 25 (2006) 24.

[3.4] D. Schmalzing et al, Anal. Chem. 70 (**1998**) 2303.

[3.5] Maxfield F. R., Curr. Opin. Cell Biol., **14** (2002) 483.

[3.6] *Biological Membrane Ion Channels: Dynamics, Structure, And Applications*, Chung S-h., Anderson O. S. and Krishnamurthy V. V., editors (Springer-verlag) 2006.

[3.7] Pathria R. K., *Statistical mechanics* (MPG Books Ltd, Bodmin, Cornwall, UK) 2005.

Subject Index

Rafts in membranes

Renewal dynamics